





## Honeybee-like collective decision making in a kilobot swarm

David March-Pons <sup>1,\*</sup>, Julia Múgica <sup>1</sup>, Ezequiel E. Ferrero <sup>2,3,4</sup> and M. Carmen Miguel <sup>2,3</sup>

<sup>1</sup>Departament de Física, *Universitat Politècnica de Catalunya, Campus Nord B4, 08034 Barcelona, Spain*

<sup>2</sup>Departament de Física de la Matèria Condensada, *Universitat de Barcelona, Martí i Franquès 1, 08028 Barcelona, Spain*

<sup>3</sup>Institute of Complex Systems (UBICS), *Universitat de Barcelona, 08028 Barcelona, Spain*

<sup>4</sup>Instituto de Nanociencia y Nanotecnología, *CNEA-CONICET, Centro Atómico Bariloche, 8400 S. C. de Bariloche, Río Negro, Argentina*



(Received 24 October 2023; accepted 1 July 2024; published 7 August 2024)

Drawing inspiration from honeybee swarms' nest-site selection process, we assess the ability of a kilobot robot swarm to replicate this captivating example of collective decision making. Honeybees locate the optimal site for their new nest by aggregating information about potential locations and exchanging it through their waggle dance. The complexity and elegance of solving this problem rely on two key abilities of scout honeybees: self-discovery and imitation, symbolizing *independence* and *interdependence*, respectively. We employ a mathematical model to represent this nest-site selection problem and program our kilobots to follow its rules. Our experiments demonstrate that the kilobot swarm can collectively reach consensus decisions in a decentralized manner, akin to honeybees. However, the strength of this consensus depends not only on the interplay between independence and interdependence but also on critical factors such as swarm density and the motion of kilobots. These factors enable the formation of a percolated communication network, through which each robot can receive information beyond its immediate vicinity. By shedding light on this crucial layer of complexity—the crowding and mobility conditions during the decision making—we emphasize the significance of factors typically overlooked but essential to living systems and life itself.

DOI: [10.1103/PhysRevResearch.6.033149](https://doi.org/10.1103/PhysRevResearch.6.033149)

### I. INTRODUCTION

Collective decision making is the process by which a group of agents makes a choice that cannot be directly attributed to any individual agent but rather to the collective as a whole [1]. This phenomenon is observed in both natural and artificial systems, and it is studied across various disciplines, including sociology, biology, and physics [2,3]. In particular, social insects have long been recognized for their fascinating behaviors, and collective decision making is no exception. An intriguing example of this can be found in the way honeybees choose their nest sites [4–7]. This specific problem has been the focus of numerous models of collective decision making in honeybees [8–13] and serves as an inspiration for our study.

The process of collective decision making can encompass a virtually infinite number of choices. For instance, in flocking dynamics, individuals often have to converge on a common direction of motion [14–18]. In such cases, achieving consensus in favor of an option is the result of a continuous process. Another category of collective decision making involves a finite and countable set of choices. Typical models in this cat-

egory require a group of individuals to collectively determine the best option out of a set of  $n$  available choices [12,19–22]. Here, the consensus-reaching process becomes a discrete problem. In real-life scenarios, examples of such decision making processes include selecting foraging patches, travel routes or candidates in a democratic election. Within this countable set of choices, consensus is achieved when a *large majority* of individuals in the group favor the same option. The threshold for what constitutes a “large majority” is typically defined by the experimenter but generally signifies a cohesive collective decision with more than 50% agreement among the individuals [20]. In these collective decision making models, each option is characterized by attributes that determine its relative desirability. For instance, in the context of selecting a potential nesting site for honeybees, these attributes could include size, distance, and vegetation type. Measures of *quality* and *cost* for each potential option encompass these attributes [5,19,23]. These two properties can be configured in multiple ways. The simplest scenario occurs when options' qualities and costs are the same for all available options, referred to as *symmetric*. In such a scenario, the group faces the challenge of breaking symmetry when selecting an option, often resulting from the amplification of random fluctuations [12,23,24]. In all other scenarios, the decision making process is influenced by the specific combination of qualities and costs among different options. For example, in cases where the cost varies among options, making it *asymmetric*, but the qualities are symmetric, the option with the minimum cost is typically considered the best choice [25]. Conversely, in situations with

\*Contact author: david.march@upc.edu

Published by the American Physical Society under the terms of the [Creative Commons Attribution 4.0 International license](https://creativecommons.org/licenses/by/4.0/). Further distribution of this work must maintain attribution to the author(s) and the published article's title, journal citation, and DOI.

asymmetric qualities but symmetric costs, the option with the maximum quality tends to be chosen [12,21,26,27].

Opinion dynamics models are proposed and developed to examine how individuals communicate and make decisions within groups. These models consist of a group of agents, each with their own instantaneous opinion or “state.” Individuals interact with one another and revise their opinions based on the opinions of others. Among the simplest models used to study collective decision making are the well-known *voter model* [28,29] or the *majority rule model* [30]. These models are limited in that they assume that all agents are equally likely to adopt either opinion. In reality, however, individuals may have different preferences, beliefs, or biases that can influence their decision making. To address this limitation, more complex models have been developed that incorporate features such as stubbornness, partisanship, and heterogeneity [22,31–34]. These models generally help to understand how opinion diversity and polarization can arise in groups, and how these dynamics might be influenced by different factors [35,36]. In recent years, the collective decision making process observed among nest-hunting honeybees has triggered the investigation of numerous collective decision making models. In these models, agents can adopt a wide variety of individual and social behaviors [10,13,26,37]. They engage in exploration to discover options, and once committed, they recruit uncommitted peers. Conversely, they may also retract their commitment and return to a neutral state or engage in cross-inhibition against opinions different from their own. Importantly, they assess the qualities of the different options, which in turn may modulate each of the aforementioned behaviors [5,38].

Taking inspiration from a simple honeybee-like collective decision making model [10], our primary focus is to determine whether autonomous minirobots, specifically kilobots, can achieve high levels of consensus for the best quality option. These robots have been extensively used in the field to design and evaluate decision making models, such as the naming game [39], as well as other comparable honeybee-inspired models [27,40,41]. These models adopt different approaches to modeling the collective decision making process; these variations and their implications will be elaborated in the following sections.

As it will emerge from our analysis, the interaction topology of agents plays a crucial role in realistic representations of collective decision making, adding complexity beyond inherent opinion dynamics. Recent studies have shown that scale-free networks offer better accuracy compared to networks based on agent proximity [42]. However, agents with constrained communication capabilities can only generate limited interaction patterns, restricting the emergence of complex network features such as clustering or small-world properties. By introducing mobility, agents can enhance their communication capabilities [43], motivating a quantitative study of the communication patterns established with this approach. Our novel aspect resides in exhaustively evaluating the interplay between the evolution of the group consensus, under the simple assumptions of our model, and its relation with the dynamic communication network.

Aside from the general insights we can gain from studying opinion dynamics with moving individuals, this scenario possesses the distinctive feature of being closer to the behavior

observed in the social animal world, where a diversity of intriguing signaling mechanisms have been previously identified [44]. In particular, crowding and clustering effects stand out as highly relevant from our study. As they were shown to be crucial for honeybees in trophallaxis [45], they might also be decisive in communication and collective decision making.

In the following, we motivate our work inspired by the honeybees’ house hunting problem in Sec. II, where we also present the particular discrete opinion-dynamics model under scrutiny. In Sec. III, we introduce our experimental study system, a *kilobots* swarm, and their emulator, KILOMBO. Sections IV and V present our main results, which combine experiments on kilobots, numerical results on the KILOMBO emulator, numerical simulations of the model on specific geometries, and their comparison to analytical results of the opinion-dynamics problem. Finally, in Sec. VI, we provide a discussion of our results and perspectives. Technical details about the model and the experimental setup are provided in Appendix A, and additional complementary analysis and data are included in Appendices C and D.

## II. MODELING THE NEST SITE SELECTION PROBLEM IN HONEYBEES

Honeybees are social insects that reside in large colonies. The way scout honeybees select new nest sites represents an interesting example of a collective decision making process that involves a combination of individual and group behaviors. In recent years, researchers have made significant progress in understanding the mechanisms behind this behavior, which is crucial for the survival and reproduction of honeybee colonies [7,46,47].

The process of collective decision making in honeybees has primarily been studied in the species *Apis mellifera*. Towards the end of spring, honeybee colonies split, with approximately two-thirds of the colony leaving the nest along with the queen in search of a new nesting site. During this process, a fraction of the swarm scouts the surroundings to gather information about potential new sites, assessing their quality based on traits such as size, food availability, or the degree of concealment [5,46]. When a scout bee discovers a promising new nesting site, it returns to the swarm and communicates information about the site fitness and location to other bees through the intricate waggle dance [19,48]. Doing so, she may recruit other scout bees that remained in the swarm to also explore—and subsequently advertise—the same location. The duration of the waggle dance is correlated with the honeybee’s perception of the site’s quality. A longer and more animated dance indicates a more suitable nest site, while a shorter and less dynamic dance corresponds to a less desirable site [49]. Consequently, high-quality sites receive longer and more frequent advertising, while low-quality sites see reduced attention, resulting in an overall increase in the number of bees visiting and dancing for high-quality sites and a decrease in those doing so for low-quality ones.

In addition to their quality, each site also has its associated cost, which represents the likelihood that a scout bee will discover the site, considering factors such as distance or concealment. This leads to the possibility that some high-quality options may go unnoticed due to their associated costs. Over

time, the dances performed by the honeybees tend to converge on a single site, and once a potential nest site has attracted a sufficient number of bees, a quorum is formed, ideally in favor of the best available option. This entire process ensures that the migrating part of the colony moves together to their new home [47].

### A. Model of a fully connected scout bee network

Several mathematical models of the honeybee nest-site selection problem have been proposed in the literature [8–13,26,37,50,51]). In particular, List, Elsholtz, and Seeley [10] introduced an agent-based model inspired by the decision making process of honeybees. This model integrates both an individual's self-discovery of potential nest sites and the existing interdependencies, which encompass interactions among bees, leading to imitation and the adoption of sites presented by other bees. The model explicitly incorporates various parameters, including the number of sites, site quality, site self-discovery probabilities, and group interdependence. Here, we adopt a very similar approach to describe the rules that govern the behavior of our kilobot robots.

The nest-site choice model proposed in Ref. [10] consists of a swarm of  $N$  scout bees that reach consensus and collectively decide on one of the potential nest sites, labeled  $1, 2, 3, \dots, k$ . Each site  $j$  has an intrinsic quality  $q_j \geq 0$  that determines the time a bee spends advertising site  $j$  through the waggle dance. At time  $t$ , a bee can either be dancing for one of the  $k$  sites (i.e., promoting it) or not dancing for any site, indicating that it is still searching for a site, observing other bees' dances, or simply resting. Formally, a vector  $x_{i,t} = (s_{i,t}, d_{i,t})$  represents the state of bee  $i$  at time  $t$ , where  $s_{i,t} = 0$  if bee  $i$  is not dancing for any site. When a bee is dancing,  $s_{i,t} = 1, \dots, k$ , indicating the site the bee is promoting, and  $d_{i,t}$  represents the remaining duration of bee  $i$ 's waggle dance. In each discrete time step (which sets the unit of time in the model), the states of bees are updated in parallel. While a bee is dancing for a site, its dance duration  $d_{i,t}$  decreases by one time unit in each time step until it reaches zero, at which point the bee stops advertising, and its state returns to the nondancing value  $s_{i,t} = 0$ . Nondancing bees have a probability  $p_{j,t+1}$  of starting to dance for site  $j$  at time  $t + 1$ . When this occurs,  $s_{i,t+1} = j$ , and the duration of the new dance is set equal to or proportional to the site quality (we have simplified the original model; for more nuanced details on this step, refer to Ref. [10]). Here we use  $d_{j,t+1} = q_j$ . The probability  $p_{j,t+1}$  estimates the likelihood of a bee finding site  $j$  and committing to advertising it. It is calculated as follows:

$$p_{j,t+1} = (1 - \lambda)\pi_j + \lambda f_{j,t}. \quad (1)$$

Here,  $\pi_j$  represents the a priori self-discovery probability of site  $j$ , i.e., the success rate of a scout bee targeting an option in the environment is simply incorporated into the system through this model parameter.  $\lambda$  denotes the bees' interdependence, and  $f_{j,t}$  represents the proportion of bees already dancing for site  $j$  at time  $t$ . As probabilities, the condition  $\sum_{j=0}^k p_{j,t+1} = 1$  must be satisfied. Similarly, the fractions  $f_{j,t}$  must satisfy a normalization condition  $\sum_{j=0}^k f_{j,t} = 1$ . Moreover, it is important to note that when  $\lambda = 0$ , the probability transitions are solely determined by  $\pi_j$ . Hence, the condition

$\sum_{j=0}^k \pi_j \leq 1$  must also be met. This inequality accounts for the possibility that bees may fail to commit to any site and remain neutral for another time step (i.e.,  $p_{0,t+1} \neq 0$ ). The interdependence parameter  $\lambda$  ranges between 0 and 1, determining the extent to which bees rely on each other to decide to dance for a site. When  $\lambda = 0$ , the probability of committing to site  $j$  depends solely on the self-discovery probability  $\pi_j$ , regardless of the proportion of bees dancing for it. Conversely, as  $\lambda$  approaches 1, the probability of committing to site  $j$  at time  $t + 1$  becomes almost entirely dependent on the proportion of bees already dancing for it at time  $t$ , denoted as  $f_{j,t}$ . In other words, a higher value of  $\lambda$  means that committing probability relies more on imitation of other bees. For further details, please refer to Appendix A 1. The self-discovery probabilities of available sites  $\pi_j$  are chosen in a way that ensures  $\sum_{j=1}^k \pi_j < 1$ , and in general, the sum does not exceed the maximum value of approximately 0.6, which corresponds to a 60% probability of independent commitment to any available nest site.

It is worth emphasizing that in this model, every bee can observe the dancing state of all other bees in the swarm, regardless of their relative separation. In this regard, the model developed by List *et al.* represents a mean-field stochastic agent-based model. Galla [52] formulated a master equation for the commitment probabilities within the same model as presented in Ref. [10]. In this formulation, he replaces the fixed duration  $d_j = q_j$  of the waggle dances with stop-dancing rates  $r_j = 1/q_j$ . Following this approach, it is possible to derive a set of nonlinear differential equations that describe the evolution of the average values  $\langle f_{j,t} \rangle$ . These equations closely align with the results obtained from the original stochastic model. Furthermore, in the long-time limit, one can analytically determine the stationary values of  $\langle f_{j,t} \rangle$  using this mean-field approximation. Appendix A 1 provides a brief description of this approach. Our model simulations implement the same stochastic method.

The nonlinear differential equations of this model resemble those describing other honeybee-inspired models [11,12,26,37], which have also been tested using kilobots [27,40,41]. However, two principal differences result in distinct behaviors that must be highlighted. First, the commitment probabilities, whether from independent discovery or recruitment do not explicitly depend on the options' qualities. Second, our model does not include cross-inhibition interactions, which are stop signals exchanged between agents holding different opinions to prompt them to revert to a neutral state and reassess their opinions.

### B. Model of quenched bee configurations

Our analysis will also consider the limiting case of random static, and generally non fully connected, configurations of agents, the *quenched configuration limit*, on which we run the same collective beelike decision model. In this limit, the global proportions  $f_{j,t}$  of agents in  $j$  state appearing in Eq. (1), as considered in the original model of List *et al.* [10], are replaced by local proportions of agents computed from a fixed list of 'neighbors' for each individual  $i$  in the group. Lists of neighbors are computed after introducing a finite communication radius  $r_{\text{int}}$  around each agent in a random quenched configuration to identify other agents in this circular area of

influence. These lists are calculated only once for each random configuration and remain unchanged during the decision dynamics.

### III. EXPERIMENTAL KILOBOT SWARM

In this study, we use a kilobot swarm as our experimental system for investigating consensus reaching and exploring the interplay between the two most important factors in the honeybee-like nest-site selection model proposed by List *et al.*, i.e., independent discovery and imitation.

Kilobots are compact open-source swarm robots, measuring 3.3 cm in diameter and 3.4 cm in height, purpose-built for the study of collective behavior [53]. Our primary goal is to experimentally investigate how the introduction of restricted robot communication capabilities (or local interactions), robot locomotion, and spatial constraints, impact consensus reaching in comparison to the beelike models introduced in Sec. II. These minirobots have previously been used to study collective decision making [27,39–41,54,55], pattern formation [56], morphogenesis [57], space exploration [43,58], collective transport of objects [59] in different experimental setups, and morphological computation and decentralized learning [60].

#### A. Kilobot' locomotion, decentralized control, and information exchange

Kilobots feature three slender, metallic legs—one in the front and two at the back. With calibrated lateral vibrating motors, they can effectively overcome static friction, enabling self-propulsion. Moreover, they have the capability to rotate either clockwise or counter-clockwise by selectively activating one of the two vibrating motors. Kilobots are equipped with an Arduino controller, memory storage, and an infrared transmitter and receiver for bidirectional communication. Within an interaction radius of up to 10 cm, as tested in complete darkness conditions (see Appendix B), kilobots can exchange messages with nearby robots, with each message carrying up to 9 bytes of information. During communication, the receiving robot assesses the intensity of incoming infrared light, enabling it to calculate relative distances to neighboring robots. Due to the observed variability in the measured communication range, we limited kilobots to consider messages within a 7 cm range. This was done to ensure homogeneity among the swarm's communication capabilities.

Each kilobot in the swarm can execute various user-programmed instructions and functions, with each processing cycle (or *loop iteration*) representing a unit of time in their dynamics. During our experiments, kilobots exist in discrete states, and their current state is visually conveyed through RGB LED lights. This makes kilobots an ideal experimental system for studying collective decision making, combining decentralized activity, limited communication capabilities and locomotion—effectively making them “programmable insects.”

We place up to 35 kilobots in a circular *arena* with a radius  $R$  delimited by rigid walls. Using an azimuthal camera, we capture the kilobot activity in accordance with the guidelines of the nest-site selection model outlined in the previous

section (see also Fig. 1). Further details about the robots technical features and about the experimental setup are presented in Appendix A 2.

#### B. KILOMBO: the kilobot swarm emulator

A useful tool to work alongside physical experiments is the kilobot-specific simulator software KILOMBO [61]. This is a C-based simulator that allows the code developed for simulations to be run also on the physical robots, removing the slow and error prone step of converting code to a different platform. In this way, we can also perform simulations using KILOMBO, to test our experimental setup and to support our results—and to complement them whenever it has not been possible to perform further experiments.

### IV. CONSENSUS REACHING IN A BEELIKE KILOBOT SWARM

In this section, we describe, both experimentally and theoretically, how the complex decision making problem of reaching strong consensus for the best-available option is solved by our beelike kilobot ensemble under different conditions. Essentially, we analyze the temporal dynamics of the proportion of bees (bots) that either advocate for one of the possible sites or remain uncommitted. We examine how these proportions evolve and eventually stabilize, while also exploring the criteria that signify the attainment of a consensus in this steady state. We compare our experimental results and KILOMBO simulations with mean-field theoretical results finding intriguing resemblances in sufficiently crowded conditions, or after long enough exploration times, but also hints towards important divergences in other plausible conditions. By implementing the nest-site selection model within a physical kilobot system, we gain the capacity to explore the consequences of more realistic robot interactions and the role of space and locality on consensus formation.

#### A. Collective decision making in kilobots

We start by running our experiments in a group of  $N = 35$  kilobots. We deploy the kilobots within a circular arena of radius  $R = 20$  cm and task them with assuming the role of scout bees. These kilobots engage in a dynamic process defined by the List *et al.* model, as elaborated in Sec. II. Each kilobot holds an internal state and displays it with a color LED. Throughout the course of the experiment, kilobots adjust their internal states based on the probabilities outlined in Eq. (1), but having only partial and individual information of the population of bees advertising each site,  $f_{i,t}$ . The computation of these values takes place after a given time step,  $\Delta t$ , of the decision process relying on the information that each uncommitted kilobot can gather from its immediate surroundings.

While the typical outcomes of the List *et al.* model dynamics have been documented in prior research [10,52], previous investigations have primarily scrutinized these developments either at the mean-field (fully connected) level [10,52] or within the context of nearest neighbor interactions within a square lattice [52]. In contrast, the present approach involves committed kilobots that move in the circular arena

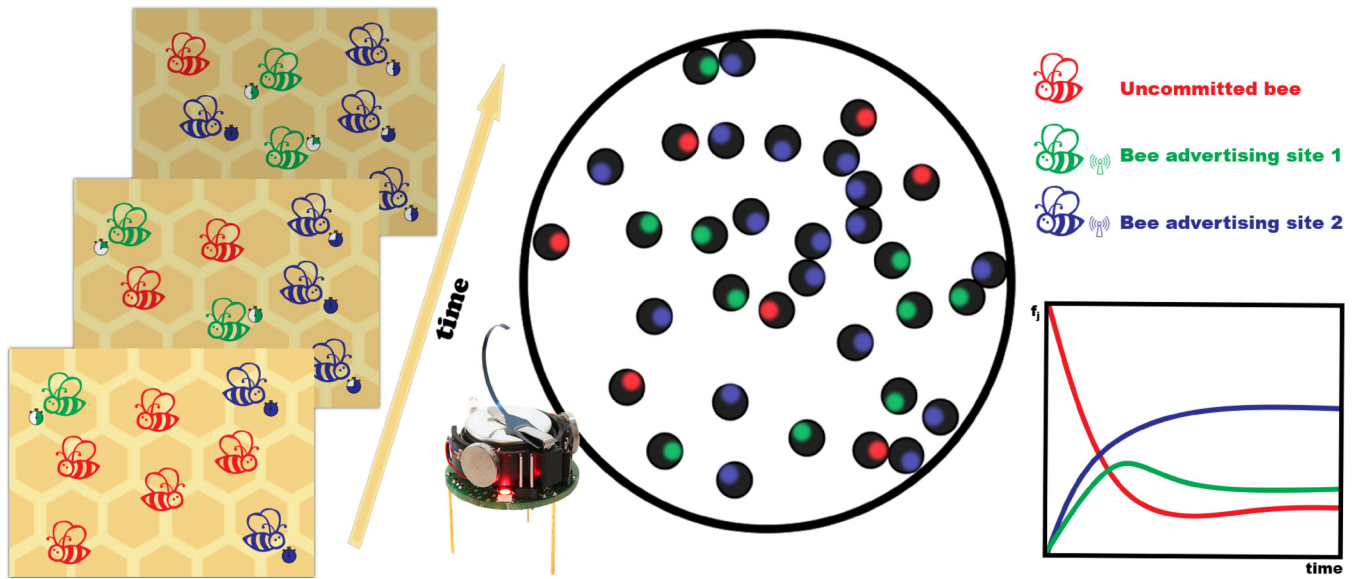


FIG. 1. Schematics of the collective decision dynamics under scrutiny. The left column represents the dynamics of the decision model: at a given instant of time committed bees are advertising their state to convince undecided bees to commit to their option. The time they spend advertising their option will be directly related to the quality they perceive for that option. As time advances a build up for the better option is expected since it is benefited from longer advertisement periods. The central column shows a schematic representation of our kilobot experiments. Each kilobot has a LED that indicates its state, either uncommitted or committed to (and advertising for) site 1 or 2. The right column displays schematically how the different proportions of bees on each state evolve in time, starting from a totally uncommitted population.

as persistent random walkers during their engagement in the advertising phase of the consensus-searching dynamics. This advertising movement results in a varying number of neighbors that they can communicate with. Such behavior mirrors that of real bees, which are known to interact with a limited number of neighbors during activities such as dancing or observing a waggle dance [62,63]. In order to correctly quantify the relevance of these factors, we first benchmark the communication capabilities of individual bots, as reported in Appendix C.

We narrow the focus of our experiments to the case of two sites: a high-quality site (designated as site 2) and a lower-quality site (referred to as site 1). The binary decision problem was chosen as the focus of our study due to its simplicity, which allows for a clearer understanding of the interplay between model parameters and the time-varying communication network. Additionally, our analysis in Ref. [64] revealed that introducing more than two options does not significantly impact the final results. At each time step kilobots are either dancing for site 1, site 2, or not advertising any site. As an extra feature towards emulating the natural behavior of honeybees, we introduce an explicit difference in the dynamics of committed and uncommitted kilobots. While kilobots advertising an option perform a persistent random walk (PRW) (see details on Appendix A 2), uncommitted kilobots, instead, come to a halt to watch other kilobot advertisements. This feature is partially inspired by the differentiation between advertising bees, which perform the waggle dance, and uncommitted bees, which adopt a more passive role.

We study both the time evolution and the steady state of the decision making experiment on our beelike kilobot system. The proportion of kilobots not advertising a site and

the proportions of kilobots dancing for sites 1 and 2, also referred to as the *dance frequencies*  $f_0$ ,  $f_1$ , and  $f_2$ , respectively, are monitored as a function of time until they stabilize and fluctuate around mean values. The duration required for the system to attain this steady state varies depending on the model's parameters. Generally, large interdependence  $\lambda$  leads to stronger majorities, while dragging out the evolution up to that state, as extensively analyzed across various scenarios in our simulations [64]. Moreover, when the competing sites have similar qualities the swarm takes longer to reach a consensus. In our experiment, site qualities are fixed to  $q_1 = 7$  and  $q_2 = 10$ ; and thus, advertising times for site 1 and 2 are equal to  $q_1 \Delta t$  and  $q_2 \Delta t$ , respectively. This choice of qualities allows us to analyze a dispute between the two available nest-site options without entering into an excessively time-consuming transient dynamics phase. Note that, as in real honeybees colonies, the kilobot swarm must make the decision for the best option within a reasonable time span, hopefully before their battery power is exhausted.

In addition, our analysis encompasses the evolution under different levels of interdependence  $\lambda$  and considers two distinct scenarios for the discovery probabilities: a symmetric case where  $\pi_1 = \pi_2$  and an asymmetric case where  $\pi_1 > \pi_2$ , favoring the lower-quality site. The specific values of  $\pi_{i,j}$  will determine the conditions under which the system can achieve consensus at different levels of interdependence. For example, in the symmetric case, this relationship is illustrated in Fig. 3. A comprehensive analysis of this interplay is provided in Ref. [64].

Figure 2(a) illustrates the dynamics of  $f_0$ ,  $f_1$ , and  $f_2$  over time, for different  $\lambda$  and for both the symmetric and asymmetric cases. The initial conditions are set as follows:

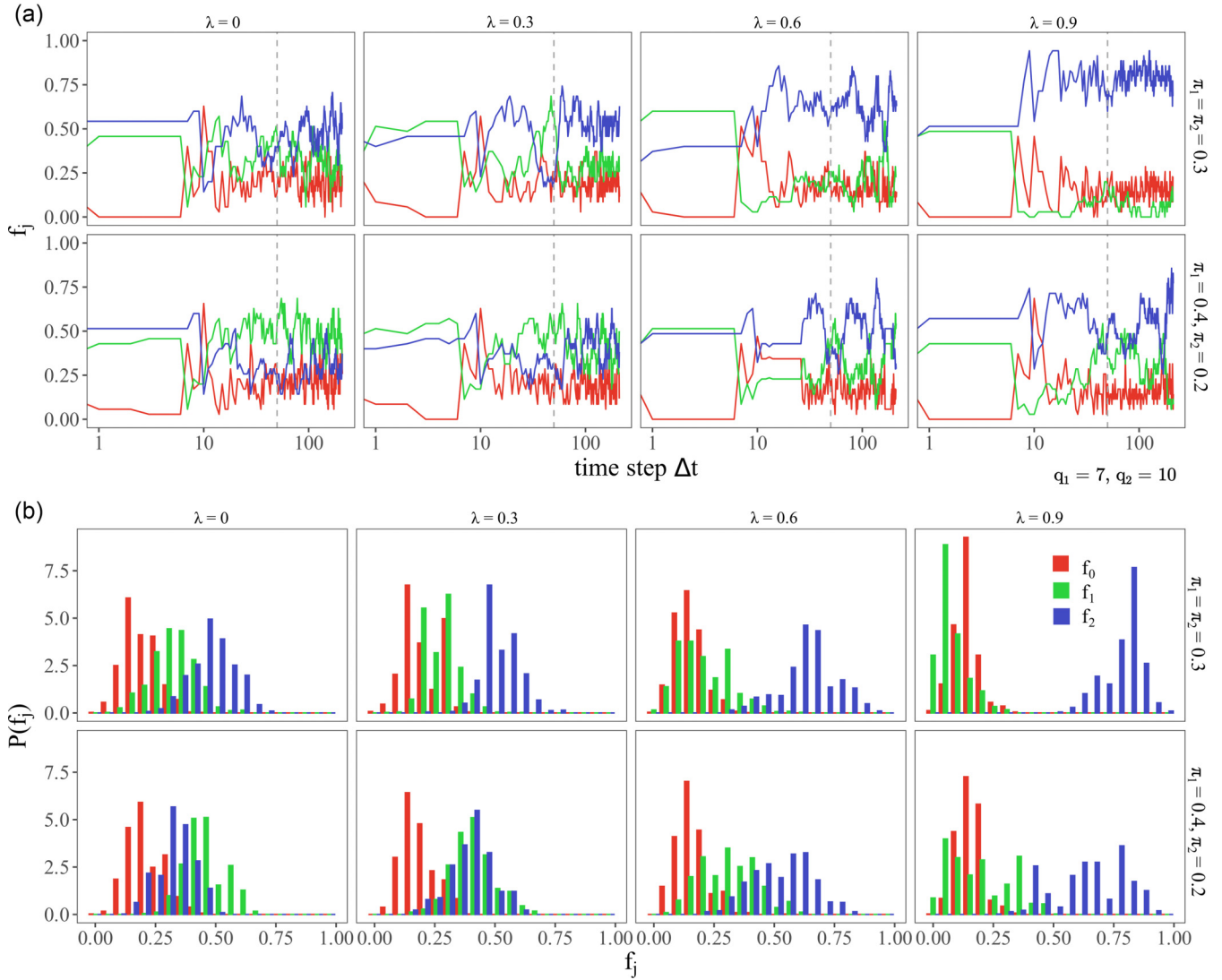


FIG. 2. (a) Proportions of kilobots  $f_j$  dancing for the different states as a function of time. Red, green and blue represent the proportion of uncommitted ( $f_0$ ) and dancers for low-quality ( $f_1$ ) and high-quality ( $f_2$ ) sites, respectively. (b) Probability density function of  $f_j$  values in the stationary state,  $P(f_j)$ . Plots correspond to symmetric (up,  $\pi_1 = \pi_2 = 0.3$ ) an asymmetric (bottom,  $\pi_1 = 0.4, \pi_2 = 0.2$ ) *a priori* discovery probabilities, with qualities  $q_1 = 7, q_2 = 10$  and interdependence parameter values  $\lambda = 0, 0.3, 0.6, 0.9$  (left to right). Five repetitions of the experiment for each  $\lambda$  were performed. The data were collected after a transient time interval of 50 time steps, indicated by the vertical gray dashed line in the temporal evolution plots.

$f_1(t = 0) = f_2(t = 0) \simeq 0.43$ , and  $f_0(t = 0) \simeq 0.14$  (i.e., approximately 15 kilobots dancing for site 1, 15 dancing for site 2 and 5 uncommitted). Other initial conditions have also been tested but, as expected, stationary results do not depend on the particular choice used in the experiments (see Supp. Fig. 1 in [65] for an example in quenched simulations). The time evolution of each population is jerky and fluctuating. This behavior is also expected and is an inherent consequence of the model dynamics, as kilobots promoting a site revert to an uncommitted state after their dancing period concludes. Additionally, due to the limited system size, these fluctuations are particularly noticeable. Nevertheless, systematic behaviors can be grasped when examining mean values and full distributions. Across all values of  $\lambda$ , there exists a transient phase in which the larger population oscillates between the

three states  $j$ , resulting in significant variations in the values of  $f_j$ . However, roughly after  $\sim 50$  time steps, a steady state is achieved, and each  $f_j$  fluctuates around its mean value. In the scenario with symmetric  $\pi$  values, irrespective of  $\lambda$ ,  $f_2$  eventually becomes the dominant population in the steady state. Moreover, increasing the interdependence parameter  $\lambda$  amplifies the difference between the proportion of kilobots dancing for the high-quality site ( $f_2$ ) and the low-quality site ( $f_1$ ). Interestingly, when we shift towards asymmetric self-discovery probabilities ( $\pi_1 > \pi_2$ ), it is observed that if  $\lambda$  is not sufficiently large, the steady state can be dominated by  $f_1$  or present a stalemate between  $f_1$  and  $f_2$ . However, increasing  $\lambda$ , the system gains the capability to favor the less accessible yet higher-quality option 2. This result aligns with other honeybee-inspired collective decision making models, where

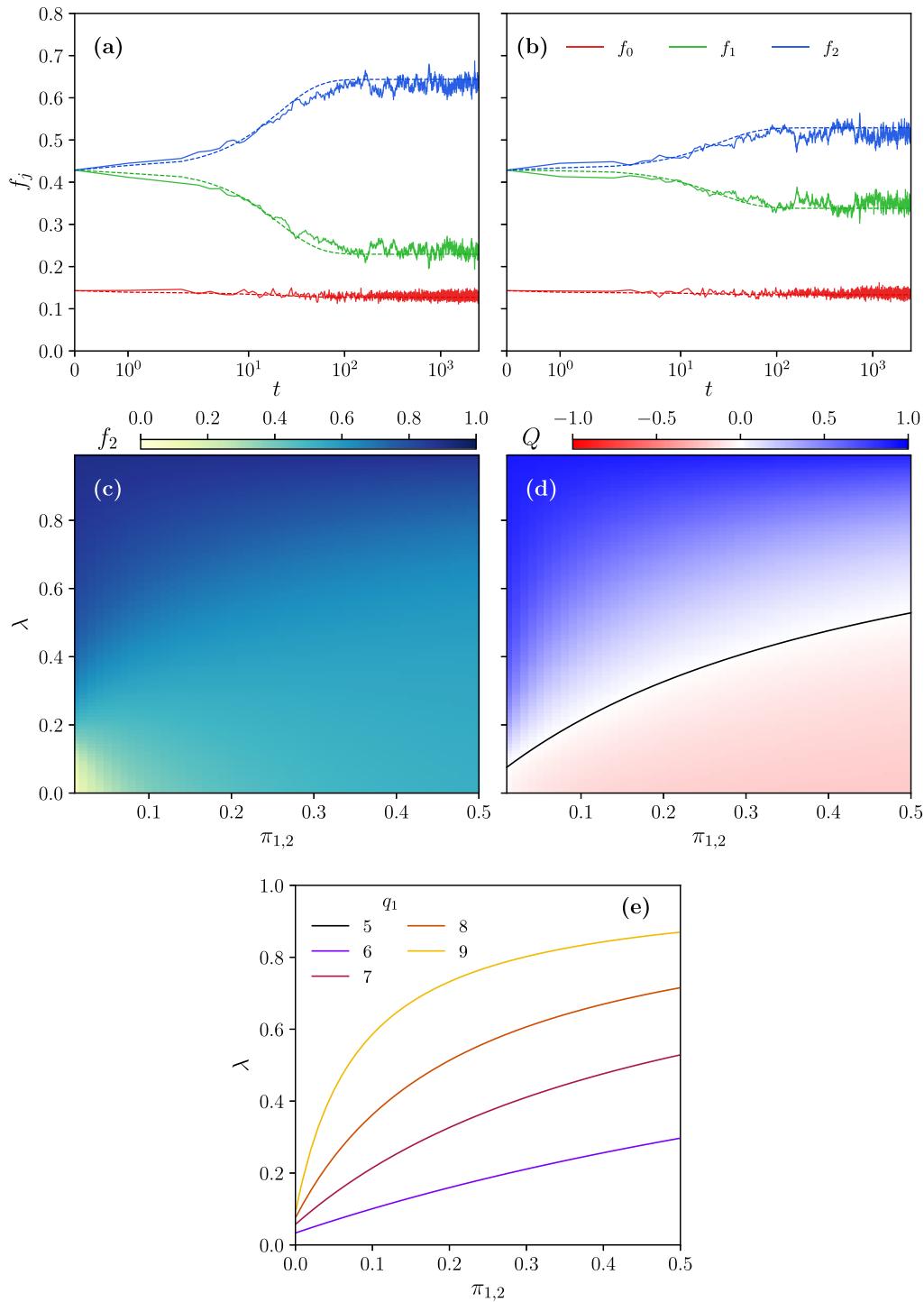


FIG. 3. [(a) and (b)] Dance frequencies  $f_0$  (red),  $f_1$  (green), and  $f_2$  (blue) as a function of time obtained from numerical simulations of the stochastic model, and from the numerical integration of the mean-field deterministic equations (smooth superimposed curves in the same color). (a) Symmetric discovery scenario with probabilities  $\pi_1 = \pi_2 = 0.3$ . (b) Asymmetric discovery scenario with probabilities  $\pi_1 = 0.4$  and  $\pi_2 = 0.2$ . Other parameters are:  $N = 35$ ,  $q_1 = 7$ ,  $q_2 = 10$ , and  $\lambda = 0.6$ . Simulations were averaged over 100 realizations. [(c) and (d)] Stationary values of  $f_2$  (c) and  $Q$  (d) in the parameter space  $(\pi_{1,2}, \lambda)$  obtained from solutions of the deterministic equations of the model. The black line in (d) corresponds to the theoretical crossover line where  $Q = 0$ . Parameters are  $q_1 = 7$  and  $q_2 = 10$ . (e) Consensus crossover lines or  $\lambda$  thresholds for consensus,  $\lambda^*$ , i.e.,  $Q(\lambda^*) = 0$  as a function of  $\pi_{1,2}$  (in the symmetric scenario,  $\pi_1 = \pi_2$ ). Colors represent different values of the low-quality site  $q_1$ , while  $q_2 = 10$  is maintained constant.

agents break the symmetry between nonequivalent options and commit to the highest quality option by enhancing the strength of social feedback [12,22].

Across all scenarios and parameter sets, there is notable dispersion in the values of  $f_j$ , resulting in broad probability distributions  $P(f_j)$  for all three  $j$ , as exhibited in Fig. 2(b). When  $\lambda$  is low, the distributions  $P(f_j)$  for all three states tend to overlap. However, with an increase in  $\lambda$ , the distributions  $P(f_1)$  and  $P(f_2)$  gradually separate from each other, eventually exhibiting significantly distinct mean values when the interdependence is at its highest,  $\lambda = 0.9$ . We quantitatively confirm this trend by measuring the Jensen-Shanon Divergence (JSD) of these probability distributions (see Supp. Fig. 2 in [65]). Specifically, the JSD tends to increase with  $\lambda$  in the symmetric discovery scenario, while in the asymmetric discovery case, it exhibits a minimum at  $\lambda = 0.3$ , after which  $f_2$  takes the lead.

While our primary focus has been on analyzing the stationary average values and their distributions around the mean, it is also valuable to examine the outcome of the decision process in more detail. For this purpose, we quantify how frequently each possible outcome (simple/strong majority for each option or draw) occurs in the experiments' stationary states. These results are displayed in Supp. Fig. 4 in [65], where the effect of  $\lambda$  becomes more evident. In the symmetric discovery scenario, the most frequent outcome is a simple majority for option 2 when  $\lambda = 0.0, 0.3$ . Further increasing the interdependence allows the system to reach strong consensus (defined in the following section). Similarly, in the asymmetric discovery scenario, we observe a shift from mostly reaching a simple majority for the bad option (when  $\lambda = 0$ ) to a strong consensus for the good option ( $\lambda \geq 0.6$ ). When  $\lambda = 0.3$ , where we observed overlapping histograms, it is equally likely for option 1 to win by a simple majority as for option 2.

### B. Consensus in numerical and analytical approaches

In the following paragraphs, we proceed with the numerical analysis of the nest-site selection problem within a fully connected system. Figures 3(a) and 3(b) present the values of the dance frequencies  $f_0$ ,  $f_1$ , and  $f_2$  as a function of time. These values are obtained from both stochastic simulations and the numerical integration of the deterministic mean-field equations, as detailed in Appendix A 1. The observed curves are qualitatively similar to the ones displayed by the evolution of the model in kilobots (as shown in Fig. 2). It is worth noting that, as for the kilobots, we use  $q_1 = 7$  and  $q_2 = 10$ . In both studied cases, whether symmetric ( $\pi_1 = \pi_2 = 0.30$ ) or asymmetric ( $\pi_1 = 0.4, \pi_2 = 0.2$ ), with the same value of  $\lambda = 0.6$ , we observe the high-quality nest site taking the lead in the steady state.

Simulations of the stochastic model display finite-size fluctuations around the mean values, whereas the numerical integration of the analytical solution produces smooth evolution curves. Notice that the analytical curves do not accurately represent the transient state at very short times, but they accurately describe the average stationary value for each parameter set. This reassuring result allows us to perform a parametric exploration of the model without the need of resource-intensive simulations.

Employing the analytical solution, we delve into the exploration of the parameter space defined by  $\pi_j$  and  $\lambda$ . We do not only assess the stationary dance frequencies  $f_j$ , but also a strong majority definition of *consensus*:

$$Q = f_2 - 2f_1. \quad (2)$$

This definition implies that there must be twice as many bees dancing for the high quality site than for the low quality site for the condition  $Q > 0$  to be met. Consequently, this represents a *large majority* consensus, i.e., a majority by a factor of 2/3 in the case there were no uncommitted bees in the system.

In Figs. 3(c) and 3(d), we present the outcome of the decision process in the symmetric scenario,  $\pi_1 = \pi_2$ . We assess both the stationary value of  $f_2$  [Fig. 3(c)] and the consensus  $Q$  [Fig. 3(d)]. The exploration of the parameter space is done by varying the values of the interdependence  $\lambda$  ( $y$  axis) for each value of the self-discovery probabilities  $\pi_{1,2}$  ( $x$  axis) (a similar parameter space exploration for the asymmetric scenario is presented in Supp. Fig. 3 in [65]). The color charts illustrate how these two metrics vary across the parameter space. We observe a smoothly varying trend indicating that the proportion of individuals dancing for the high quality site  $f_2$  increases along with the interdependence parameter  $\lambda$ , regardless of the specific value of  $\pi_1$  and  $\pi_2$ . This phenomenon arises from bees placing more reliance on the opinions of their peers, and as  $\lambda$  increases, it enhances the reinforcement for the best possible option. Contrarily, when both independent discoveries ( $\pi_1 = \pi_2$ ) increase simultaneously, there is a relative decrease in the number of bees dancing for site 2. This means that as  $\pi$  values increase while keeping  $\lambda$  constant, more advertisements are motivated by independent discoveries rather than by opinion sharing. Consequently, when  $\pi_1 = \pi_2$ ,  $f_1$ , the population of bees dancing for site 1 increases at the expense of site 2, hindering overall consensus. In the extreme case of  $\pi_1 = \pi_2 = 0.5$ , this translates in consensus never being achieved (i.e.,  $Q < 0$ ) if the interdependence parameter is lower than  $\sim 0.5$ . The black line depicted in Fig. 3(d) corresponds to the strong consensus crossover  $Q = 0$ , computed using the analytical solution. A system with a set of parameters given by points below this line will never find strong consensus, but it will do for a set of parameters given by a point above. In other words, after surpassing a  $\pi_{1,2}$ -dependent  $\lambda$  *threshold*,  $\lambda^*$ , the system crosses over to a strong consensus state,  $Q > 0$ , and the strength of this consensus intensifies with increasing interdependence. The region of nonconsensus expands as  $\pi_{1,2}$  values grow, thereby narrowing the range of interdependence values that lead to consensus.

Certainly, the ‘‘critical’’ line  $\lambda^*(\pi_1, \pi_2)$  is contingent upon the values of qualities  $q_1$  and  $q_2$  as well. In Fig. 3(e), we represent  $\lambda^*$  as a function of  $\pi_1 = \pi_2$ , maintaining a fixed value of  $q_2 = 10$  while exploring different choices of  $q_1$ . We observe that when  $q_1$  is markedly smaller than  $q_2$ , particularly when  $q_1 \leq q_2/2$ , the region of no strong consensus basically disappears, i.e., the swarm is able to choose the high quality site with strong majority, allowing for consensus even when  $\lambda = 0$ . On the other hand, when  $q_1$  increases and approaches the value of  $q_2$ , the competition between sites intensifies. Consequently, a higher value of  $\lambda$  becomes necessary to counteract the influence of the discovery probabilities.



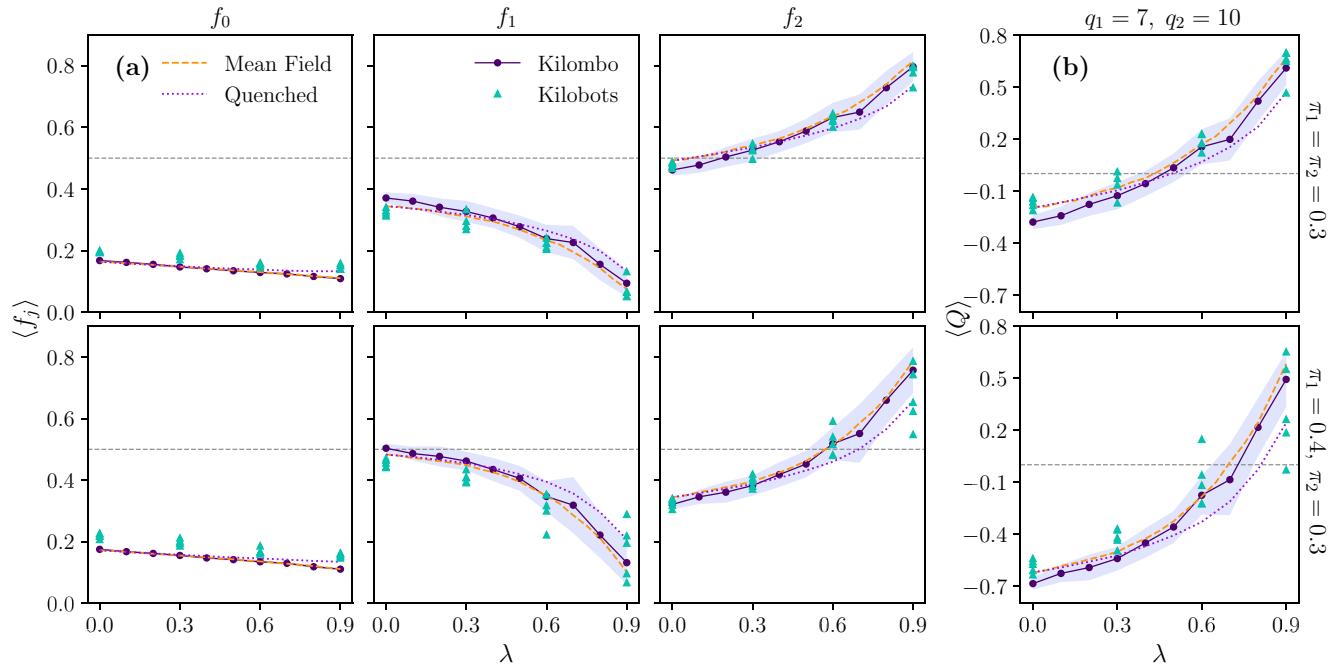


FIG. 4. Stationary dance frequencies and consensus as a function of interdependence. (a) Average frequencies  $\langle f_0 \rangle$ ,  $\langle f_1 \rangle$ , and  $\langle f_2 \rangle$  and (b) Average consensus  $\langle Q \rangle$  as a function of  $\lambda$  for symmetric (up) and asymmetric (bottom)  $\pi_i$  for physical kilobots, and for simulations using KILOMBO, quenched configurations and fully connected networks. Triangles: Mean values from experiments of  $N = 35$  kilobots (5 repetitions per parameter combination). Solid purple line with points: Mean values from KILOMBO simulations with  $N = 35$  bots averaged over 50 repetitions. Shaded area: KILOMBO standard deviation. Dashed orange line: mean values from simulations of the fully connected model with  $N = 35$  bots averaged over 100 repetitions. Dotted pink line: mean values from quenched configurations with  $N = 35$  bots averaged over 100 repetitions.

For a given  $\lambda$  and  $\pi_{1,2}$ , the quality difference necessary for the system to achieve consensus is directly proportional to the mean quality of the options [64], and thus the  $\lambda^*$  crossover lines depend solely on the options' relative quality difference. This observation is in agreement with Weber's Law of perception, as reported in previous studies on similar collective decision making models [11,66]. Unlike these models, ours does not require incorporation of discovery or recruitment rates that depend on the options' qualities to adhere to this fundamental law. Finally, when the qualities and discovery probabilities of available options are equal, both options become equivalent, transforming the decision problem into a symmetry-breaking task between identical options. Here, the main distinction from other honeybee-inspired models [37,41]—the presence or absence of cross-inhibition interactions—becomes crucial. In scenarios where external information is continually introduced through independent commitment transitions, cross-inhibition has been identified as a vital mechanism for breaking decision deadlocks [27,67]. In contrast, our model system can resolve deadlocks differently by adapting its behavior upon deadlock detection, either by halting exploration (effectively setting  $\pi_\alpha = 0$ ) or by maximizing social interactions (i.e.,  $\lambda = 1$ ). A detailed analysis of these parameter limits is provided in Ref. [64].

### C. Comparison between experiments and simulations

We would like to quantitatively compare the steady-state averages in kilobots with those obtained from the modeling

approaches. Our goal is to distinguish the emerging properties of the real system, which involves restricted communication capabilities, and moving individuals, in comparison to the fully connected approximations made in mean-field solutions. To enhance this comparison, we utilize KILOMBO [61], the kilobot's emulator, to conduct complementary simulations under the same experimental conditions. On the other hand, alongside the fully connected stochastic model simulations, we also incorporate the steady-state results obtained from simulations with quenched configurations of bots running the same collective decision making model.

Figure 4 displays the average stationary values of the dance frequencies  $\langle f_0 \rangle$ ,  $\langle f_1 \rangle$ ,  $\langle f_2 \rangle$ , and the consensus  $\langle Q \rangle$  as functions of the interdependence parameter  $\lambda$  for both symmetric and asymmetric scenarios defined by the same self-discovery probabilities  $\pi_i$ , and site-quality values  $q_1 = 7$  and  $q_2 = 10$ , considered previously. Consistently, the primary trend is similar across all approaches: at small values of interdependence  $\lambda$ , the majority of the population gravitates towards the high-quality site (2) in the symmetric case. Conversely, it aligns with the low-quality site (1) when asymmetric self-discovery probabilities favor it. In this case, there is no consensus for the higher quality option, and  $Q$  assumes negative values. As  $\lambda$  increases,  $\langle f_1 \rangle$  decreases while  $\langle f_2 \rangle$  increases for both the symmetric and asymmetric scenarios. Moreover,  $\langle f_1 \rangle$  and  $\langle f_2 \rangle$  exhibit similar functional trends but in opposite directions, resulting in the stationary value of  $\langle f_0 \rangle$  remaining nearly independent of  $\lambda$ . When examining the stationary average of the strong consensus parameter  $\langle Q \rangle$ , we observe a smooth

transition from nonconsensus to consensus as  $\lambda$  varies. This is rather a crossover more than a phase transition, but it can be precisely identified. Notably, in scenarios with symmetric discovery probabilities, consensus is achieved at smaller  $\lambda$  values compared to asymmetric scenarios. This is because there is less introduction of independent discoveries for the low-quality site, leading to less misleading information that needs to be discarded through communication.

Now, let's delve into a quantitative comparison of the different approaches, going beyond the observed consistency in the data. First, it is noteworthy that the stationary values obtained from physical kilobots closely match those from KILOMBO simulations, even within the standard deviation (represented by shaded areas). This alignment underscores the reliability of the emulator in complementing real measurements. More remarkably, both experimental and emulator results closely align with the mean-field results. This coincidence might be less expected, and we will discuss the reasons behind it for the chosen set of parameters. These findings suggest that mobile kilobots, as they interact with their local environment, can effectively sample the system's state and transmit information throughout, almost as if they were fully connected, achieving collective decision making comparable to mean-field fully connected individuals. We will test this hypothesis in the next section. However, it's worth noting that this agreement is not perfect. While  $\langle f_j \rangle$  and  $\langle Q \rangle$  values are nearly identical for all approaches at low values of  $\lambda$ , some differences become noticeable after an interdependence value of approximately  $\lambda \sim 0.5$ . In this range, quenched configurations exhibit higher  $\langle f_1 \rangle$  and lower  $\langle f_2 \rangle$  values than the fully connected system. Furthermore, for high  $\lambda$  we observe a broader scattering of the experimental results, especially in the asymmetric discovery scenario. As a consequence of these variations, we observe a lower consensus value compared to the fully connected case. In the asymmetric scenario, particularly for high interdependence ( $\lambda \gtrsim 0.7$ ), quenched simulations show a crossover to consensus at a substantially higher value of  $\lambda$  compared to the fully connected case. Additionally, experiments exhibit significant fluctuations in stationary consensus, with some realizations failing to achieve consensus or closely resembling the quenched results.

In summary, in a high enough interdependent system, the experimental results displayed in Fig. 4 demonstrate that mobile individuals, such as kilobots moving in space and integrating information over time, are capable of achieving high consensus values comparable to fully connected systems. The exact threshold depends on model parameters such as quality differences and self-discovery probabilities. Quenched configurations, characterized by fixed neighbor lists for interactions, help us assess the importance of kilobots' movement and mixing under experimental conditions. Despite the limited communication range of kilobots, our hypothesis is that their mobility enables information to spread in a manner that the outcome of the decision making problem becomes similar to mean-field results. However, in quenched configurations conditions, local consensus for the low-quality option may emerge, diminishing the chances of attaining strong consensus for the best-quality option. In agreement with Raoufi *et al.* [55], we observe that the network structure significantly influences the accuracy of the final decision. A greater

communication range results in a better-connected network, characterized by a higher average degree, leading to improved accuracy. Furthermore, by varying the weighting factor of social interactions, i.e., the interdependence parameter, we recognize its significance in collective decision making processes with limited communication.

## V. INFORMATION SPREADING IN THE KILOBOT SWARM

In this section, we provide a more detailed analysis of the information spreading taking place in our kilobot swarm as they play the beelike decision making process. Various models of state-contagion dynamics have been explored using self-propelled particles [68–71]. The relationship between agents' states, their mobility, and packing fraction gives rise to different physical phenomena. For instance, motility-induced phase separation occurs at low densities [71], while segregation between agents with opposing opinions is observed in [70]. We take a simpler approach by considering a model that does not include correlations between movement patterns and the underlying opinion dynamics. Instead, our aim is to investigate under which circumstances consensus reaching in motile physical kilobots can be almost as effective as in an idealized mean-field-like communicating system. This is achieved by allowing them to gather local information over a limited temporal window.

When analyzing the data presented in Fig. 4, and observing the consistency between the fully connected approach and the results obtained from kilobots (both experimental and emulated) across a wide range of values for  $\lambda$ , our primary hypothesis centers around the crucial role played by the kilobot density and the kilobot motion in allowing them to form a connected communication network [39,42,43]. Through a percolated communication network, each kilobot can receive information beyond its immediate surroundings, set by the infrared sensor capabilities, and spread it throughout the system.

We investigate the occurrence of this percolation transition in the kilobot intercommunication network, to understand its relation with consensus formation. This intercommunication network can be represented as a complex network [72,73], where nodes correspond to kilobots, and where two nodes are connected by an edge if the corresponding kilobots are within an Euclidean distance smaller than their interaction radius. Since infrared communication in kilobots is approximately isotropic, the network is undirected, meaning that if bot  $i$  interacts with bot  $j$ , bot  $j$  would also interact with bot  $i$ . Consequently, these networks are based on proximity. Although they do not have the information transfer advantages of long-range networks with scale-free degree distributions [42], the kilobots' mobility enhances their communication and consensus reaching capabilities [43]. Due to the agents' mobility, this proximity network is time-varying (see Supp. Fig. 6 in [65] and video 4).

In Ref. [39], the authors used kilobots and the *naming game* to explore the importance of percolating communication networks. However, despite involving moving robots, the percolation threshold discussed there was related to instantaneous interactions between robots. Here, we consider time-integrated networks that result from information exchanges occurring within a short temporal window  $\Delta t$  while

our robots move. This is why our percolation threshold  $\eta^*$  includes a movement component over this temporal window. Our percolation analysis demonstrates that at robot densities well below the instantaneous percolation threshold, where information percolation would not occur in corresponding static configurations and thus strong consensus would not be achieved, the movement of agents over the time interval  $\Delta t$  facilitates consensus formation.

We therefore characterize the percolation transition in the kilobot communication network examining standard quantities such as the mean communication cluster size, the emergence of a giant component, the cluster size distributions, or the average connectivity, as a function of the kilobots communication radius and their advertising time window (some details and complementary analysis are left for Appendix D). Finally, we study how this transition impacts the outcome of the decision making problem.

### A. Communicating clusters of kilobots

Leveraging numerous spatial configurations generated in KILOMBO simulations, we examine the cluster structure within the kilobot communication network. A cluster is defined as a connected component in which nodes can be reached from one another via continuous paths of adjacent edges [72]. In computational terms, a kilobot is considered part of the same communication cluster as a focal kilobot if it resides within a circular region centered on the focal kilobot with a radius of  $r_{\text{int}}$ , denoting the effective interaction radius. This recursive process identifies all clusters and their sizes in each spatial configuration.

The mean-cluster size, denoted as  $\langle S \rangle$ , is a key parameter in the analysis of cluster structures. It shares similarities with transport coefficients like magnetic susceptibility and specific heat and plays a crucial role in the geometrical percolation process [74]. This quantity measures the fluctuations within the cluster size distribution and aids in detecting a continuous percolation transition, where the communication network shifts from having only small isolated clusters of kilobots to forming a large, connected communicating component. The percolation transition occurs as a function of the interaction radius  $r_{\text{int}}$  at a fixed kilobot density, or as a function of density for fixed values of  $r_{\text{int}}$ . Both quantities can be combined into a single control parameter  $\eta = Nr_{\text{int}}^2/R^2$ , which measures the effective area covered by kilobots. Note that we are referring to an effective communication area rather than to the physical area occupied by the kilobot swarm. Thus the percolation transition takes place at a threshold value  $\eta^*$  of this control parameter.

The mean-cluster size is defined as [74]

$$\langle S \rangle = \frac{\sum' s^2 n(s)}{\sum' s n(s)}, \quad (3)$$

where,  $n(s)$  represents the number of clusters of size  $s$ , i.e., composed of  $s$  kilobots, and summations  $\Sigma'$  exclude the *giant component* of the network,  $S_{\text{max}}$ , which is the largest cluster observed in a given configuration. In finite systems,  $\langle S \rangle$  exhibits a characteristic peak, instead of diverging, at the percolation threshold [72,74].

Figure 5 displays the mean-cluster size and average giant component obtained from KILOMBO simulations of kilobots as they execute PRW trajectories. Specifically, we calculate the mean-cluster size characterizing their communication network integrated over the exploratory, or advertising, time window  $\Delta t$ . This integration considers the total number of communication contacts accumulated over the time step  $\Delta t$ . We examine the communicating clusters for various time windows  $\Delta t = 0, 400, \text{ and } 800$  (measured in kilobot's loop iterations) or equivalently, for  $\Delta t = 0, 4.12, \text{ and } 8.24$  seconds, and for two different system sizes, with  $N = 35$  and 492 kilobots. At this point, we want to increase the system size while maintaining a constant kilobot density, so the arena size is adjusted to keep a constant value of  $n = N/\pi R^2 = 0.028$  bots/cm<sup>2</sup>. Later on, we will also vary the kilobot density for completeness.

The mean-cluster size  $\langle S \rangle$  varies with the interaction radius  $r_{\text{int}}$ , as shown in Fig. 5(a), exhibiting a peak at a threshold radius denoted by  $r_{\text{int}}^*$ . For comparison and consistency check, we have included a clustering analysis for random quenched configurations of kilobots using the same sizes and density conditions. Notice that indeed the data corresponding to  $\Delta t = 0$  (instantaneous snapshots) closely resemble the results obtained from the quenched configurations. The small discrepancies are due to the existence of short range spatial correlations in configurations obtained from the kilobots' dynamics, which includes collisions. Such correlations are absent in the quenched configurations.

The threshold radius  $r_{\text{int}}^*$  undergoes a notable shift towards smaller values as  $\Delta t$  increases. Larger values of  $\Delta t$  correspond to increasing intercommunication opportunities due to the kilobot's advertising dynamics (see Appendix C), and therefore to higher number of contacts in the communication network. Thus a larger  $\Delta t$  translates into a reduced percolation threshold radius, beyond which a giant communication component forms. Figure 5(b) shows the average size of the giant component as a function of  $r_{\text{int}}$  for the same values of  $\Delta t$ . As the giant component approaches saturation, the communication network has percolated. In particular, after an advertising time window of  $\Delta t = 800$  loops (8.24 s) in the experimental system with  $N = 35$  kilobots, the percolation threshold shifts from approximately  $6.5 \pm 0.1$  cm to  $r_{\text{int}}^* = 3.75 \pm 0.25$  cm, very close to the minimum distance between a kilobot pair ( $r_e \approx 3.3$  cm) due to excluded volume interactions (see Supp. Fig. 5 in [65]).

Interestingly, at the finite-size percolation threshold, the normalized distribution  $P(s) = n(s)/n_{\text{tot}}$  of cluster sizes exhibits a power-law decay,  $P(s) \sim s^{-\tau}$ , persisting up to a cutoff value that depends on system size. This scaling behavior is shown in Fig. 6, where we observe a fair consistency with an exponent value  $\tau \simeq 2.055$  expected for continuous percolation in  $D = 2$  [74]. Beyond the cutoff, the decay becomes usually much steeper. A percolation analysis based on physical contact between particles is reported in Ref. [69], where motile particles interact in order to synchronize their internal oscillators. In that study, physical percolation occurs at higher packing fractions, leading to significant many-body interactions in the system. As a result, they obtain a slightly smaller exponent for the power-law decay of the cluster size distribution at the percolation transition,  $\tau \simeq 1.7$ . It would be

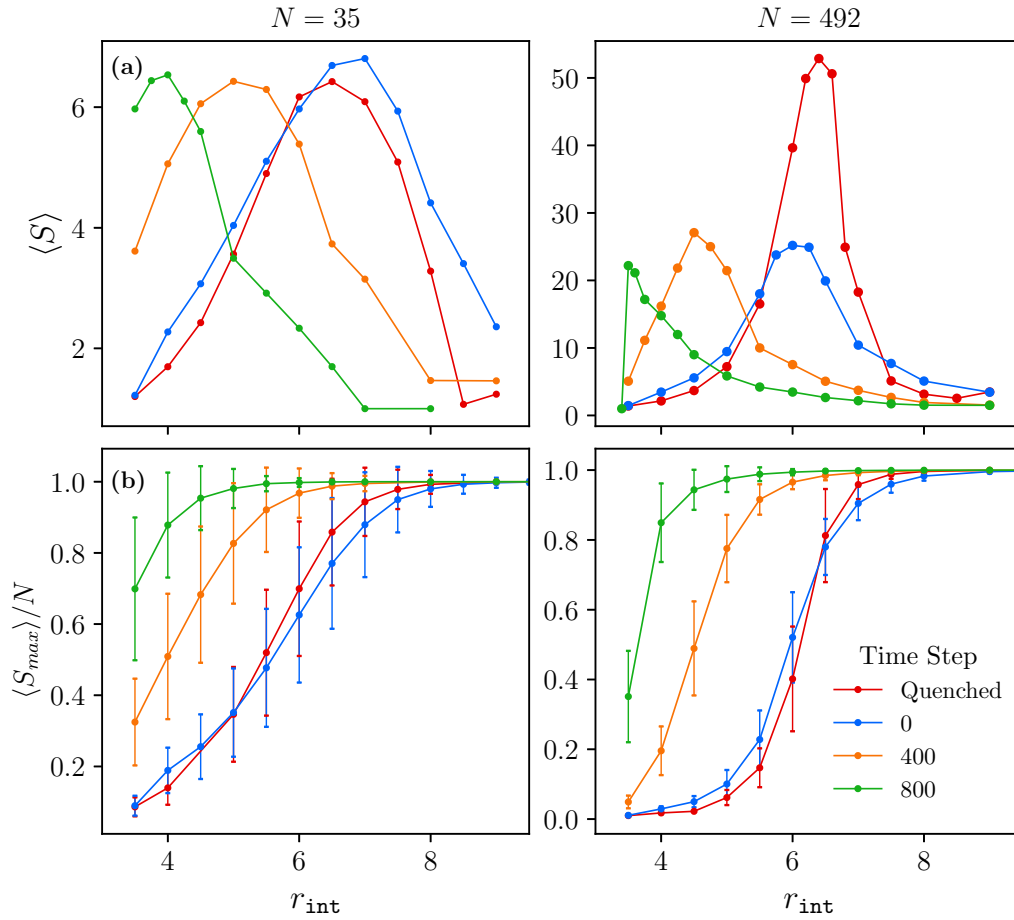


FIG. 5. (a) Mean-cluster size  $\langle S \rangle$  and (b) average giant component normalized by the system size  $\langle S_{\text{max}} \rangle / N$  as a function of the interaction radius  $r_{\text{int}}$  for KILOMBO configurations integrated over different time steps  $\Delta t = 0, 400$ , and  $800$  kilobot loop iterations, and for random quenched configurations. The left panel shows the results for  $N = 35$  kilobots, while the right panel shows results for  $N = 492$  kilobots and the same number density  $n = 0.028$  bots/cm<sup>2</sup>.

intriguing to explore whether a similar exponent emerges in our experiments under similar crowding conditions. However, such analysis is currently beyond the scope of the present work.

In summary, increasing values of  $\Delta t$  yield lower percolation threshold values for the pairwise interaction radius, as a result of the kilobot exploratory dynamics. By moving, bots increase their average number of communication contacts favoring the widespread of information through the system. Given that in the experimental set-up discussed in the previous section we have  $N = 35$  kilobots with an approximate infrared communication radius of 7 cm, exploring their neighborhood for a time window of  $\Delta t = 800$  loops ( $\Delta t = 8.24$  s), we can conclude that the kilobot dynamics is effectively generating a percolating infrared communication network, which enables information exchange at the system-wide scale, or as in a fully connected mean-field like scenario.

### B. Crowding effects in consensus reaching

Once we understand the importance of communication among seemingly sparse and distant individuals, while they integrate remote sensing over a short temporal window as they disperse in space, we can return to the study of the

main collective decision making observables in less favorable conditions. In particular, it is now evident that the quantitative values of the dance frequencies, including uncommitted individuals ( $f_0$ ) and those promoting specific sites ( $f_1, f_2$ ), as well as the consensus parameter  $Q$ , will depend on the swarm's effective crowding.

In this section, we explore how the number density of kilobots  $n = N/\pi R^2$ , their communication distance  $r_{\text{int}}$ , and their sensing time  $\Delta t$  influence the consensus outcome, considering different values of the interdependence parameter  $\lambda$ . Eventually, the dimensionless control parameter  $\eta = Nr_{\text{int}}^2/R^2$ , measuring the effective area covered by kilobots, will determine the formation and strength of consensus as a function of the beelike model parameters  $\lambda, q$ , and  $\pi$ .

To illustrate crowding effects, we start by systematically analyzing the influence of the communication range  $r_{\text{int}}$  on the decision making process in the quenched configuration approximation. Figure 7 displays the stationary values of the dance frequencies  $f_0, f_1$ , and  $f_2$  as a function of the interdependence parameter  $\lambda$ . The data are presented for various values of the interaction radius  $r_{\text{int}} \in [3, 12]$  cm, represented by different colored curves. We fix the number density of kilobots to  $n = 0.028$  bots/cm<sup>2</sup>, nest-site qualities  $q_1 = 7$  and  $q_2 = 10$ , and independent discovery probabilities  $\pi_1 = \pi_2 =$

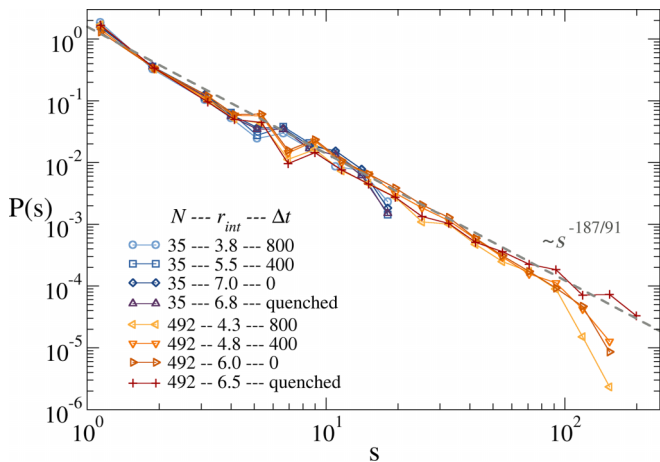


FIG. 6. Probability distribution of cluster sizes  $P(s)$  at the percolation transition for KILOMBO and quenched kilobot simulations. The plot shows results for two system sizes with  $N = 35$  and  $N = 492$  and the same kilobot number density  $n = 0.028$  bots/cm<sup>2</sup>. For  $N = 35$ , the corresponding percolation thresholds are  $r_{int}^* \simeq 3.8$  cm (KILOMBO configurations integrated over  $\Delta t = 800$  loops),  $\simeq 5.5$  cm (KILOMBO configurations integrated over  $\Delta t = 400$  loops),  $\simeq 7.0$  cm (instantaneous KILOMBO configurations with  $\Delta t = 0$ ), and  $\simeq 6.4$  cm (random quenched configurations). For  $N = 492$ , one finds  $r_{int}^* \simeq 4.3$  cm (KILOMBO configurations integrated over  $\Delta t = 800$  loops),  $\simeq 4.8$  cm (KILOMBO configurations integrated over  $\Delta t = 400$  loops),  $\simeq 6.0$  cm (instantaneous KILOMBO configurations with  $\Delta t = 0$ ), and  $\simeq 6.5$  cm (random quenched configurations). The gray dashed-line corresponds to a power law decay with an exponent  $\tau = 187/91$  characterizing the cluster distribution in 2D continuous percolation. It emphasizes the compatibility of our results with a percolation transition.

0.3 to match the experimental conditions. For comparison, we also include the expected stationary values in the mean-field approximation, represented by dotted-dashed lines, as well as the limiting case where bots remain completely isolated, a trivial limit of the decision making process that one can easily work-out analytically, shown as black dashed lines.

The dependency of these zero-interaction curves on  $\lambda$  arises from the fact that increasing  $\lambda$  limits self-discovery [as one can deduce from Eq. (1)] without any information exchange taking place.

For the largest interaction radius, the stationary values of  $f_j$  tend towards the mean-field predictions. As discussed previously, beyond an interaction radius of approximately 6.5 cm, we have a percolating communication network that allows information exchange among nearly all bots in the system. Consequently, for all interaction radii greater than this threshold ( $r_{int}^* \simeq 6.5$ ), the  $f_j$  curves roughly match the mean-field results, and completely stabilize around  $r_{int} \sim 10$  cm. Conversely, as the interaction radius decreases from  $r_{int}^*$ , the  $f_j$  values significantly deviate from mean-field predictions, particularly for higher values of the interdependence parameter  $\lambda$ , when communication capabilities become crucial. When  $r_{int} \leq 3$  cm, due to excluded volume effects, there are no bots within the intercommunication distance (since each bot has a diameter of 3.3 cm, touching robots cannot interact), and the stationary values of  $f_j$  follow the isolated kilobots limit.

When  $\lambda = 0$ , the value of the interaction radius becomes irrelevant, and all curves converge to the same point, known analytically from the mean-field approximation solution of the model. The same analysis can be carried out by fixing an interaction radius  $r_{int}$  and changing the number of bots  $N$  in a fixed-size arena. The final outcome will be the same, as it is shown in Fig. 8.

Figure 7 reveals an interesting phenomenon occurring at low  $r_{int}$ : for high values of  $\lambda$ , the values of  $f_1$  exceed the zero-interaction limit bound. This is because in small isolated clusters present in such quenched configurations, at high values of  $\lambda$ , one opinion may dominate for long periods without the other entering into the discussion, thus being overrepresented. Both populations are influenced by this effect, but it is more noticeable for  $f_1$  as it is expected to diminish when  $r_{int}$  increases, while  $f_2$  is expected to grow. This overshooting effect occurs at the expense of the uncommitted population; hence, the pronounced decrease of  $f_0$  for low  $r_{int}$  and high  $\lambda$  can be attributed to this phenomenon.

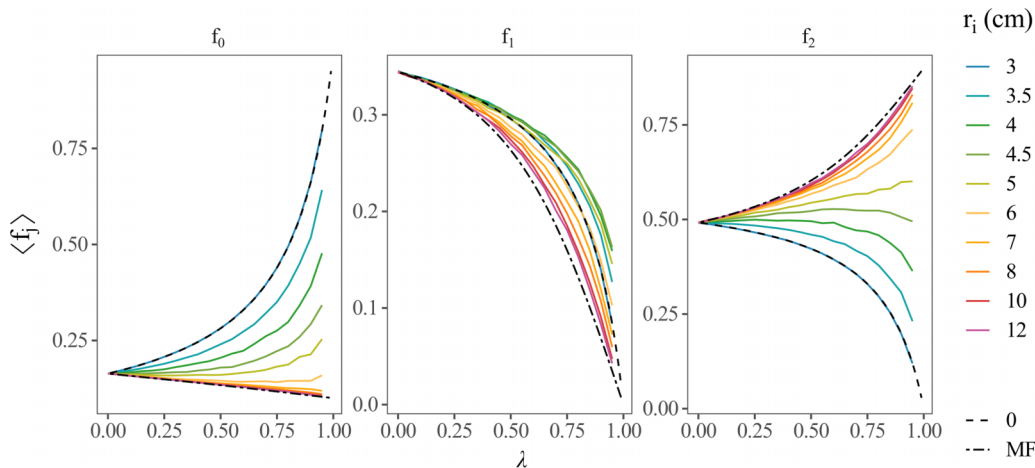


FIG. 7. Stationary proportions of bots dancing for the different sites as a function of the interdependence parameter  $\lambda$  for different values of the communication radius  $r_{int}$ . Color curves correspond to simulations of the model on random quenched configurations. Dot-dashed lines show the result of the mean-field approximation, and dashed lines display the limit case of isolated bots, i.e.,  $r_{int} = 0$ .

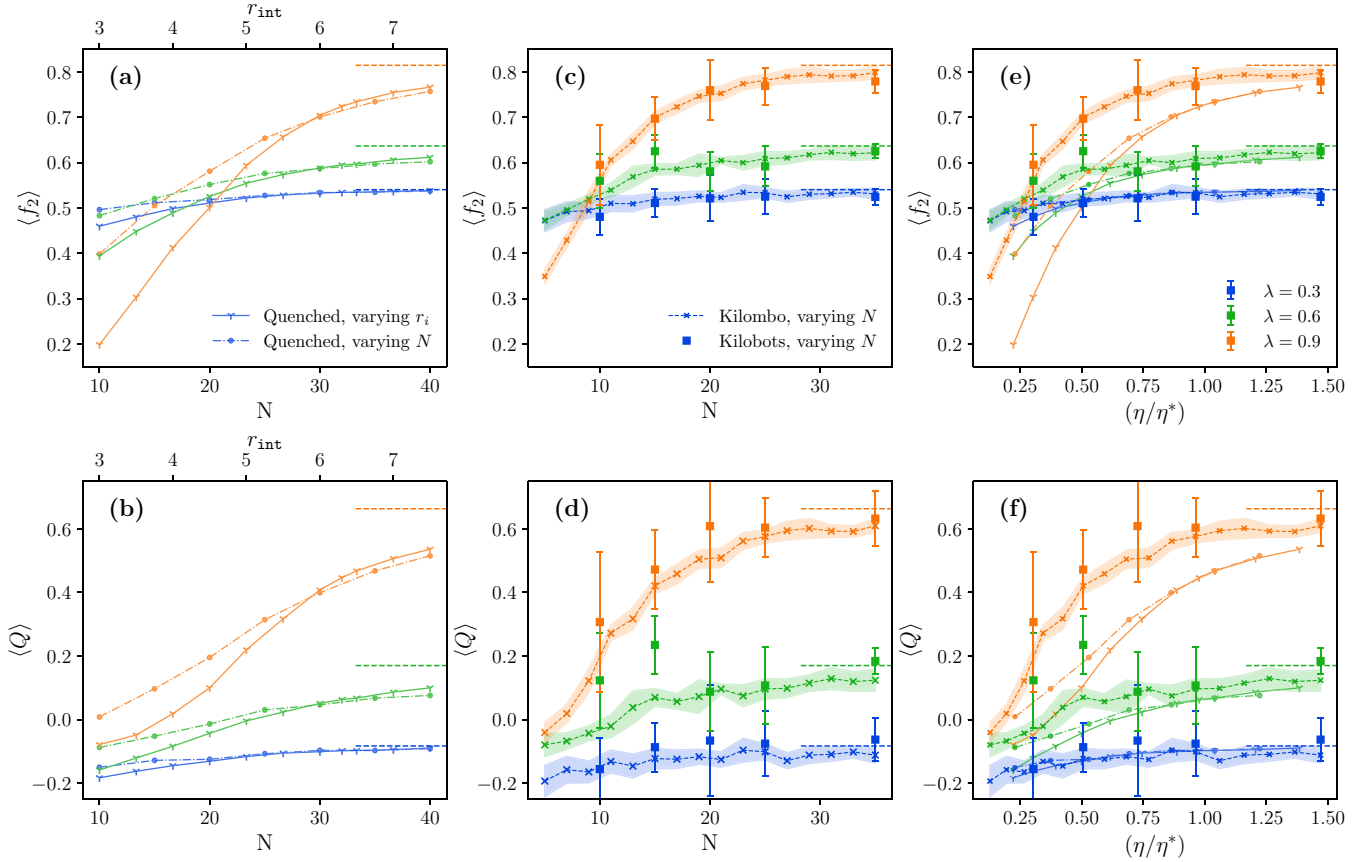


FIG. 8. Stationary dance frequency for the high quality site  $\langle f_2 \rangle$  (top) and consensus parameter  $Q$  (bottom) as a function of the crowding control variables  $N$ ,  $r_{\text{int}}$ , and  $\eta$ . (a) and (b) show results obtained from (i) different ensemble sizes  $N$  and a fixed value of  $r_{\text{int}} = 6.5$  cm (dashed-dot lines with dot symbols), (ii) from different interaction radii  $r_{\text{int}}$  and a constant number of  $N = 35$  bots (continuous lines with Y-shaped symbols), both in the quenched position approximation; (c) and (d) show results obtained from (iii) KILOMBO simulations (crosses) varying  $N$  and (iv) kilobot experiments for different ensemble sizes,  $N = 10, 15, 20, 25, 35$  (square symbols). All simulations/experiments have been conducted for three contrasting values of the parameter  $\lambda = 0.3, 0.6, 0.9$  (blue, green, and orange lines, respectively). (e) and (f) show the stationary values depicted in (a), (b) and (c), (d), now as a function of the percolation parameter  $\eta$  rescaled by the corresponding percolation threshold  $\eta^*$ .

Finally, we investigate the impact of crowding on mobile PRW kilobots at different densities by changing the number of bots  $N \in [5, 35]$  in the same arena of radius  $R = 20$  cm. Based on the analysis presented in the previous section and in Fig. 7, we anticipate that kilobots, with the ability to move and to gather information over a temporal period  $\Delta t$ , will achieve better communication and consequently higher consensus levels compared to quenched configurations in the same conditions.

Figure 8 provides a comparison of stationary averaged values of  $f_2$  and  $Q$  in experiments, KILOMBO simulations, and simulations using random quenched configurations. We consider three contrasting values of the interdependence parameter  $\lambda$  in the symmetric probability discovery scenario. In Figs. 8(a) and 8(b), we show the impact of working with different kilobot numbers  $N$  or restraining their communication radius  $r_{\text{int}}$ . Plots 8(a) and 8(b) show the comparison between varying  $N$  or  $r_{\text{int}}$  in the quenched approximation. Furthermore, plots 8(c) and 8(d) show experimental results for varying number  $N$  of kilobots contrasted with KILOMBO simulations. In all cases the average values of  $f_2$  and  $Q$  increase gradually with  $N$  until they reach a plateau for  $N > N^* \sim 30$  kilobots.

The plateau values lie very close to the asymptotic mean-field results for each value of  $\lambda = 0.3, 0.6,$  and  $0.9$ . This means that even for lower number densities than the ones considered in the experiments shown in Sec. IV (where  $N = 35$ ), the system seems to be able to perceive global information about dancing frequencies and to achieve consensus values very similar to mean-field results. This is, again, a signature of the formation of a percolating communication network as a function of kilobot density. On the contrary, the consensus parameter for very small ensemble sizes is below zero for the three contrasting values of the interdependence parameter considered, and thus strong consensus for the best quality option is not achieved in such poorly communicated swarms.

Within error bars, the stationary values of  $f_2$  and  $Q$  obtained from experiments with  $N \in [5, 35]$  kilobots match those from KILOMBO simulations. Furthermore, moving kilobots achieve higher levels of consensus than quenched configurations with the same number of robots. This is particularly evident for small groups of kilobots and high enough values of interdependence. We have seen that the PRW motion of kilobots enhances the transmission of information and, thus, shifts the percolation transition towards smaller values of

the coverage parameter  $\eta$ , by either decreasing the threshold value of  $r_{\text{int}}^*$  or, equivalently, by reducing the number  $N^*$  of kilobots required to observe the percolation transition. This shift can be clearly seen by comparing Figs. 8(a), 8(b) and 8(c), 8(d), for both experimental and KILOMBO simulation results of moving kilobots that establish new contacts over a given time window of  $\Delta t = 800$  loops.

In Figs. 8(e) and 8(f), the same data are now represented in terms of the dimensionless control parameter  $\eta = Nr_{\text{int}}^2/R^2$ , measuring the effective area covered by kilobots, rescaled by the corresponding percolation threshold  $\eta^*$  calculated in each case. Despite the rescaling by  $\eta^*$  yields qualitatively similar dependencies on the control parameter for all the cases considered, moving kilobots slightly outperform the consensus reached in quenched conditions at high values of interdependence. This is probably due to the existence of enhanced spatial correlations below the percolation transition. Such correlations appear as a result of their characteristic dynamics, which includes the possibility of exhibiting collisions and jams and, therefore, the formation of slightly larger clusters. This fact improves the formation of strong consensus for the best quality site around the percolation transition, when  $\lambda$  is high enough, as large clusters chiefly vote for the same option, enhancing  $f_2$  while hindering  $f_1$ .

Overall, these results underscore the significance of information spreading facilitated by agents' mobility, interaction time, and interdependence. They highlight the capability of robot swarms to achieve consensus successfully even under less-than-ideal conditions. Identifying the percolation transition allows us to pinpoint the specific combination of parameters that lead to nearly mean-field performance. In contrast to Ref. [39], our study relies on mobility networks integrated over a short temporal communication window, emphasizing that agents' mobility and communication capabilities within this timeframe play a pivotal role in fostering strong consensus in natural systems.

To conclude this section, we would like to mention that the percolation threshold is affected by finite size effects. In particular, the percolation correlation length for finite systems can only attain a maximum value

$$\xi_{\text{max}} \sim (\eta^*(N) - \eta_{\infty}^*)^{-\nu} \sim N^{1/d_f}, \quad (4)$$

where  $\nu = 4/3$  and  $d_f = 91/48$  are the critical exponents for the correlation length and the fractal dimension [74], respectively, for continuous percolation in  $D = 2$ . Therefore, for the percolation threshold, one expects that

$$\eta^*(N) \sim \eta_{\infty}^* + CN^{-\frac{1}{d_f}}, \quad (5)$$

where  $C$  is an arbitrary constant. From this expression, we expect that the percolation radius for different kilobot densities scales as

$$(r_{\text{int}}^*(N))^2 \sim (r_{\text{int}}^{\infty})^2 + C'N^{-(\frac{1}{d_f}+1)} \quad (6)$$

with  $(r_{\text{int}}^{\infty})^2 \sim 0$ . Indeed, in the case of quenched configurations we obtain  $r_{\text{int}}^{*2} \sim N^{-1.21}$ , while in the case of kilobots we obtain  $r_{\text{int}}^{*2} \sim N^{-1.26}$  (see Supp. Fig. 5 in [65]). These exponents, although slightly smaller than the continuous percolation expectation, are another indicator of a percolation process taking place in the communication network.

## VI. DISCUSSION

We have investigated the problem of the nest-site selection process of honeybee swarms using kilobots, i.e., minimalist robots that can mimic their consensus-reaching behavior. Kilobots engage in a honeybee-like collective decision model while they move in the experimental arena, and we analyze how adding space and local interactions affects consensus reaching in (a simplified variant of) the model proposed by List and coworkers in 2009 [10]. In order to rationalize our experimental results, we use an analytical approach, obtained from the deterministic differential equations governing the dynamics in the mean-field approximation [52,64], as well as numerical simulations in both fully connected and random quenched kilobot configurations. Furthermore, we complement the limited statistics of our experiments with simulations using the KILOMBO emulator of the kilobot dynamics.

The problem of reaching consensus decisions in a decentralized manner, i.e., the need of targeting the best among many available options when many agents participate in the decision process and none of them exerts particular influence—displays great complexity and beauty and relies on information pooling and on communication. In our experiments, self-discovery and imitation, i.e., *independence* and *interdependence*, are both essential ingredients in collective decision making. Despite the differences between our studied model and other honeybee-inspired models such as [11,12,26,37], we similarly highlight the importance of social interactions in collective decision making processes. We find that high levels of interaction enable the swarm to more accurately identify the highest-quality option, especially when the qualities of options are close or when discovery probabilities (uncorrelated with site qualities, unlike the aforementioned works) are large. The primary distinction between our model and others in the literature is the absence of cross-inhibition [27,67]. As a result, if symmetry breaking is required to resolve deadlocks, it can be achieved through a simple adaptation in behavior—specifically, by ceasing exploration. For an extensive analysis of the parameter space and dynamics of symmetry breaking, refer to Ref. [64]. Finally, in line with recent studies that also use decentralized robot swarms [27,39–41,54], we have demonstrated that kilobot swarms are capable of reaching such a complex consensus decisions collectively in a decentralized manner even in far from ideal conditions.

The resulting quantitative strength of the final consensus depends not only on the prescriptions of independence and interdependence characterizing the underlying opinion dynamics but also on the resulting communication network produced by the agents' mobility. This approach allows us to extend previous studies on swarm decision making, which have already considered the topology of interactions [39,42,55], by explicitly examining the time-varying and time-integrated communication network along with its percolation transition. We have observed that, within the bounded decision making space, the temporal window during which agents can interact, in addition to the communication range and bot density, controls the percolation of the communication network. At percolation, our data for cluster size distributions, as well as for the finite-size scaling of the percolation threshold itself, are consistent with standard continuous percolation critical exponents in two dimensions. Besides underscoring mobility

as a crucial factor in order to foster consensus within a poorly swarm [39] (i.e., below an static percolation threshold), our approach acknowledges the significance of agents' mobility within a short temporal communication window in real, natural or robotic, systems for identifying a dynamic communication percolation threshold. Specifically, the interaction patterns generated by mobility reduce the necessary interaction range or system density compared to static networks.

Thus we have concluded that an effective communication coverage, which integrates communication range, agent density, and motility, controls the transition, enhancing the effective information transfer of a network based on proximity interactions rather than on long-range scale-free degree distributed interactions [42]. This facilitates the achievement of consensus in the model dynamics. Without the communication coverage reaching a critical threshold, the consensus is poor or nonexistent, and high enough interdependence, or imitation, turns out to be crucial for building up strong consensus for the best-available option in poorly communicating swarms. This is even more the case in asymmetric scenarios where self-discovery favors suboptimal options.

Our study contributes to the understanding of the complexity of decentralized decision making by interacting and moving agents, establishing the main variables to pay attention at. Simultaneously, it raises a warning on the interpretation of simple agents models solved at the mean-field level or simulated in static regular grids. This is especially relevant when considering the limited communication capabilities of real systems, such as the social insects that inspire our research.

It is important to note that our analysis assumes a temporally invariant scenario, where options, discovery probabilities, and qualities remain constant. However, it would be interesting to investigate alternative scenarios where agents encounter a changing environment, such as options with fluctuating qualities or the appearance of new options. In such cases, a more constrained topology of interaction may prove to be a beneficial asset for the swarm, as observed in recent studies (e.g., Refs. [54,75]).

We believe that the swarm robotics approach, whether through conducting real experiments or simulations with realistic emulators, is better suited for studying the capabilities of complex real systems. This is because it allows for the introduction of imperfect, yet to some extent uncontrollable, motion, communication, and synchronization capacities. By extensively describing their advantages and limitations, their capabilities and uncertainties, we give a recipe on how to address them as a swarm when playing a democratic game. Alongside the literature on collective decision making in robotic swarms, we hope that our work will encourage further analysis from a physics perspective on *minirobots as programmable social matter*.

#### ACKNOWLEDGMENTS

We acknowledge financial support from projects PID2022-137505NB-C21, PID2022-137505NB-C22, PID2019-106290GB-C21 and PID2019-106290GB-C22, funded by Spanish MCIN/AEI/10.13039/5011000110033 and ERDF/EU. D.M.-P. acknowledges support from the

fellowship FPI-UPC2022, granted by Universitat Politècnica de Catalunya. E.E.F. acknowledges support from the Maria Zambrano program of the Spanish Ministry of Universities through the University of Barcelona and PIP 2021-2023 CONICET Project N° 0757. We would like to thank Ivan Paz for professional help in the design of the KILOCOUNTER tracking software and Quim Badosa for technical assistance in kilobot experiments.

## APPENDIX A: METHODS

### 1. Deterministic solutions of the mean-field model

In Ref. [52], T. Galla provided an analytical approach to List *et al.* model using a simple alteration of the original model. As mentioned in the main text, Galla replaces the state variables  $(s_{i,t}, d_{i,t})$  by  $s_{i,t}$ , and introduces a dance abandonment rate  $r_j$  for each site such that  $\langle r_j \rangle \sim q_j^{-1}$ . Following the mathematical details provided in Ref. [52], one can arrive to a set of deterministic differential equations that describe the time evolution of the system. For each site  $j = 1, \dots, k$ :

$$\dot{\langle f_{j,t} \rangle} = (1 - \rho(t))[(1 - \lambda)\pi_j + \lambda\langle f_{j,t} \rangle] - r_j\langle f_{j,t} \rangle, \quad (\text{A1})$$

where  $\rho(t) = \sum_{\alpha=1}^k \langle f_{\alpha,t} \rangle$ . Equation (A1) can be numerically integrated for any fixed choice of parameters. Nevertheless, an expression for the stationary points of these equations can be found as the solution of  $k$  coupled quadratic equations, obtained by setting  $\dot{\langle f_{j,t} \rangle} = 0$ ,

$$f_j^* = \left[ \frac{r_j}{1 - \rho^*} - \lambda \right]^{-1} (1 - \lambda)\pi_j \quad j = 1, \dots, k. \quad (\text{A2})$$

In order to solve this system of equations that unavoidably depends on the stationary value  $1 - \rho^* = f_0^*$ , one can combine the  $k$  equations to solve first a closed equation for  $f_0^*$ :

$$f_0^* = 1 - (1 - \lambda) \sum_{j=1}^k \left[ \frac{r_j}{f_0^*} - \lambda \right]^{-1} \pi_j. \quad (\text{A3})$$

Equation (A3) has  $k + 1$  roots that can be found by solving the equation numerically or by rearranging it as a  $(k + 1)$ th degree polynomial in  $f_0$ . Some of these roots lead to unphysical solutions with  $f_0^* > 1$ . From the remaining valid solutions with  $f_0^* \leq 0$ , only one leads to valid ( $f_j^* \leq 1$ ) and linearly stable solutions for the rest of dance frequencies. Stochastic simulations and the integration of Eq. (A1) confirm the stability of this result.

The extreme cases  $\lambda = 0$  and  $\lambda \rightarrow 1$  have simpler solutions. First, setting  $\lambda = 0$  in Eq. (A3) leads to a simpler solution,

$$f_0^* = \frac{1}{1 + \sum_{m=1}^k \pi_m q_m}, \quad (\text{A4})$$

that we can use to compute the result for the rest of the dancing frequencies. Using Eq. (A2), we obtain

$$f_j^* = \frac{\pi_j q_j}{1 + \sum_{j=m}^k \pi_m q_m}. \quad (\text{A5})$$



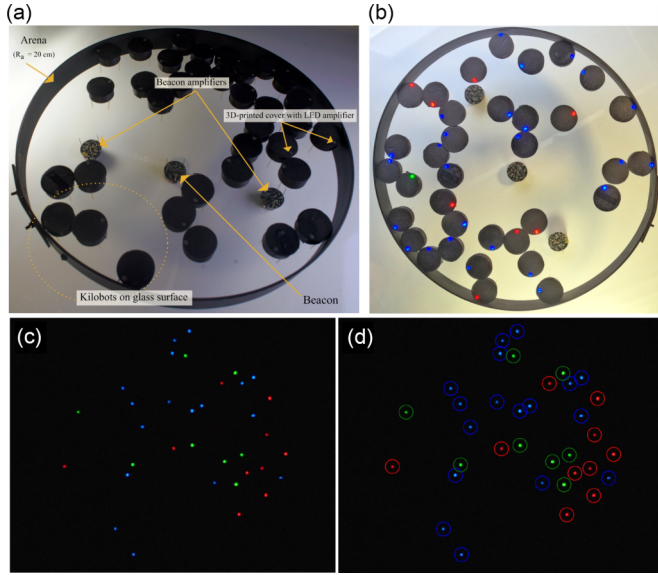


FIG. 9. (a) Kilobots experimental setup. (b) kilobots dynamics as described in Sec. II (see videos 2 and 3 in Supp. Mat. [65]). Each kilobot is covered by a custom 3D-printed case that enhances visual on the led light and allows for tracking. (c) A single frame showcasing a group of 35 kilobots, each identified by their colored light, dancing for site one (green), site two (blue), or not dancing for any site (red). (d) The frame in (c) processed using the KILOCOUNTER software.

When  $\lambda \rightarrow 1$ , due to the extreme reliance on interdependence, the site with a greater quality will be finally dominating the whole system, leaving no agents committed to the other sites and only a small quantity of uncommitted agents. Assuming that  $q_k > q_{k-1} > \dots > q_1$ , we can impose that  $f_1^* = \dots = f_{k-1}^* = 0$ , and using Eq. (A2), we find the following stationary solution:

$$f_0^* = r_k, \quad f_1^* = \dots = f_{k-1}^* = 0, \quad f_k^* = 1 - r_k. \quad (\text{A6})$$

This result is validated by simulations, or after solving the deterministic equations at high values of  $\lambda$ . A linear stability analysis confirms that this solution is the only stable solution in the limit  $\lambda \rightarrow 1$  [64].

## 2. Kilobots experimental setup

Kilobots have been instrumental in collective behavior research [53]. Kilobots execute user-programmed functions in *loops*, and the loop duration varies based on the complexity of the operations. In our case, kilobots perform a persistent random walk while gathering information, estimating population frequencies, computing transition probabilities, and indicating their commitment state during each loop. For our experiments, we set up a workspace with kilobots moving on a glass surface held 15 cm above a whiteboard melamine base. On the melamine base, we place a central kilobot that acts as a beacon to enhance synchronization of the kilobots' internal clocks, alongside two additional kilobots that amplify the beacon signal. Our typical setup is illustrated in Fig. 9(a)—see also video 2 in Supp. Mat. [65]. Synchronization is important

TABLE I. Number of realizations of the kilobot experiments for each experimental condition defined by  $N$  and  $\lambda$ .

$\lambda$	N					35
	10	15	20	25		
0.3	10	6	5	5	5	
0.6	10	7	5	5	5	
0.9	10	5	5	5	5	

to coordinate concurrent processes, such as those involved in the collective decision model.

Our kilobots operate on a persistent random walk (PRW) dynamics, characterized by straight motion segments with durations that follow an exponential distribution, averaging around  $\sim 3.8$  seconds. Upon completing each straight movement, the kilobots randomly choose to turn left or right. To prevent clustering at the arena's borders, the PRW includes discrete wide turning angles, enabling the kilobots to turn away from the border more effectively. The kilobots randomly select between short turns and long turns, with equal probabilities.

Groups of 10 to 35 kilobots move as PRWs in a circular arena with a 20 cm radius. After transmitting and receiving messages, and gathering information from their local environment, during a time step  $\Delta t$ , typically 800 loop iterations or approximately 8.24 seconds, kilobots update their state according to the model dynamics, and consequently “dance for” either site 1 (low quality), site 2 (high quality), or for no site, displaying such individual state in their LED (red for nondancing, green if dancing for site 1, and blue if dancing for site 2).

To prevent our group of kilobots from clustering at the wall of the circular observation area, their random dynamics was configured with discrete wide turning angles to promote quicker turning away from the border. Turning times consist of approximately  $\sim 2.8$  seconds ( $125^\circ$ ) or  $\sim 5.8$  seconds ( $251^\circ$ ), and their moving forward states last approximately  $\sim 3.8$  seconds. To better identify the kilobots' states, we covered each kilobot with a custom 3D-printed black casing, leaving only the LED light visible, as seen in Fig. 9(b).

We recorded the kilobots dynamics and LED states using a digital camera with a spatial resolution of  $1920 \times 1080$  pixels and a temporal resolution of 25 frames per second. Each recording session lasts typically 30 minutes. To automatically count the number of kilobots dancing for each site, we extract images at each time step  $\Delta t$ , and we make use of the KILOCOUNTER software, specifically developed for our work [76]. Kilocounter identifies and counts colored blobs in these recordings, allowing us to analyze kilobot behavior, as shown in Figs. 9(c) and 9(d). To facilitate the tracking, videos are recorded in a dark setting (see video 3 [65] for an snapshot of the experiments).

Table I sums up the amount of experiments conducted for each condition, defined by the system size  $N$  and the interdependence parameter  $\lambda$ . Due to the time consuming process of conducting the experiments, the number of realizations is limited.

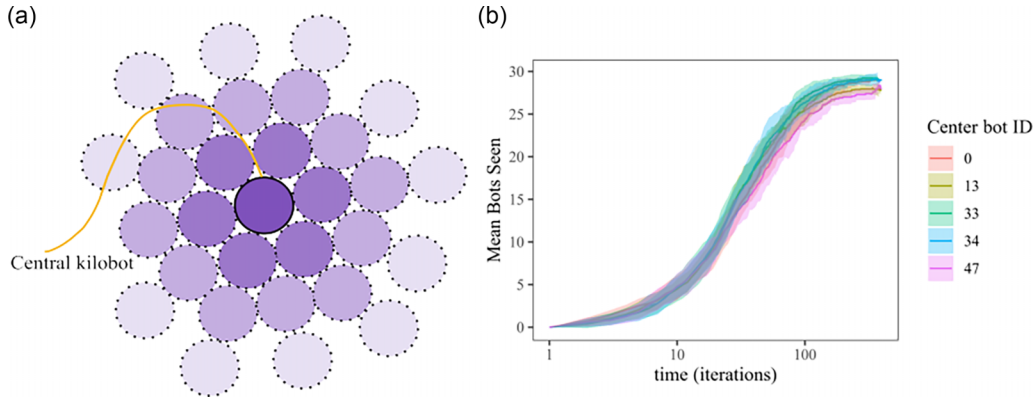


FIG. 10. (a) Representation of the experimental conditions under which we tested the kilobots’ ability to sense their surroundings up to an approximate distance of 3 kilobot diameters (approx. 10 cm). (b) Mean number of kilobots seen by a central kilobot as a function of time. Different kilobots, identified by their bot ID, were used in the test.

**APPENDIX B: KILOBOT COMMUNICATION CAPABILITIES WITHIN THE EXPERIMENTAL SETUP**

In the methods section, we outlined that the kilobot experiments were conducted under complete darkness to facilitate tracking of the LED lights for subsequent analysis of the system state. We briefly assess the communication capabilities of the kilobots under these conditions.

Physical kilobots are typically designed to interact within a range of 7 to 10 cm, as noted in previous studies [53]. However, Valentini *et al.* observed a communication range of up to 20 cm for two isolated kilobots when placed on a glass surface under light conditions [40]. We confirmed this observation by conducting the same test.

Under more crowded conditions and in complete darkness, we have studied how a central kilobot can sense the number of kilobots in its surroundings up to an approximate distance of 3 kilobot diameters, or approximately 10 cm. Figure 10 depicts the experimental setup (A) and results for different kilobots (B). We observe that in the long run, kilobots are able to sense their entire surroundings, consisting of 29 other kilobots. In the following section, we further study the kilobots communication capabilities while performing the same dynamic behavior as in the collective decision making experiments.

**APPENDIX C: KILOBOTS DETECTED OVER A TIME-STEP**

In the study of opinion dynamics, understanding how individuals interact to make decisions is crucial. Kilobots gather information from their neighbors and then act accordingly. We want to know how many other bots are detected by a kilobot during a time step.

We thus implement an algorithm for a bot to communicate, at each time step, the number of bots seen over the previous time step. We will run this algorithm on uncommitted, non-dancing bots, while the dancing bots (promoting either site 1 or site 2) perform PRWs. First, we check that the maximum number of kilobots detected by an uncommitted bot (during a time step  $\Delta t = 800$  loops) is around 15, in the 20 cm arena with 35 kilobots running the nest-site selection model. We

restrict the count to bots seen within an interaction radius of  $\sim 7$  cm, about 2 kilobots’ body lengths. This is possible by filtering for the infrared signal intensity. We then divide the number of bots detected during a time step  $\Delta t$  in four intervals, and assign each interval a color: red (0–3 bots), green (4–7 bots), blue (8–11 bots) and white (12–15 bots). At each time step, uncommitted bots flush their LEDs according to this color code, and we count the numbers with the KILOCOUNTER software. We perform five repetitions of 210 time steps (about 30 minutes each) to gather statistics (over  $\sim 20\,000$  counts) (see video 1 [65] for a demonstration of the experiment).

Figure 11 shows in a boxplot the ratio  $D_{n,m}$ , which represents the proportion of kilobots detecting from  $n$  to  $m$  neighbor kilobots during  $\Delta t$ . Most kilobots only detect 0–3 other bots, or 4–7, during a time step. In other words, undecided bots detect on average  $2.92 \pm 2.50$  bots during each  $\Delta t$ .

Additionally, we used the KILOMBO simulator, confirming that the number of kilobots detected per  $\Delta t$  was consistent with our experimental results. Figure 12(a) shows the distribution of bots detected by a focal kilobot  $i$  in  $\Delta t$ ,  $B_{i,\Delta t}$ .

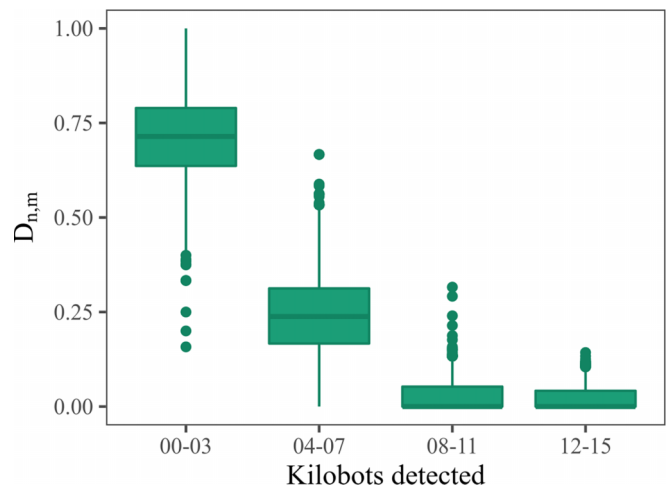


FIG. 11. Kilobots detected over a time step  $\Delta t$  in experiments. The boxplots show the proportion of kilobots detecting from  $n$  to  $m$  neighbors for four different  $(n, m)$  ranges.

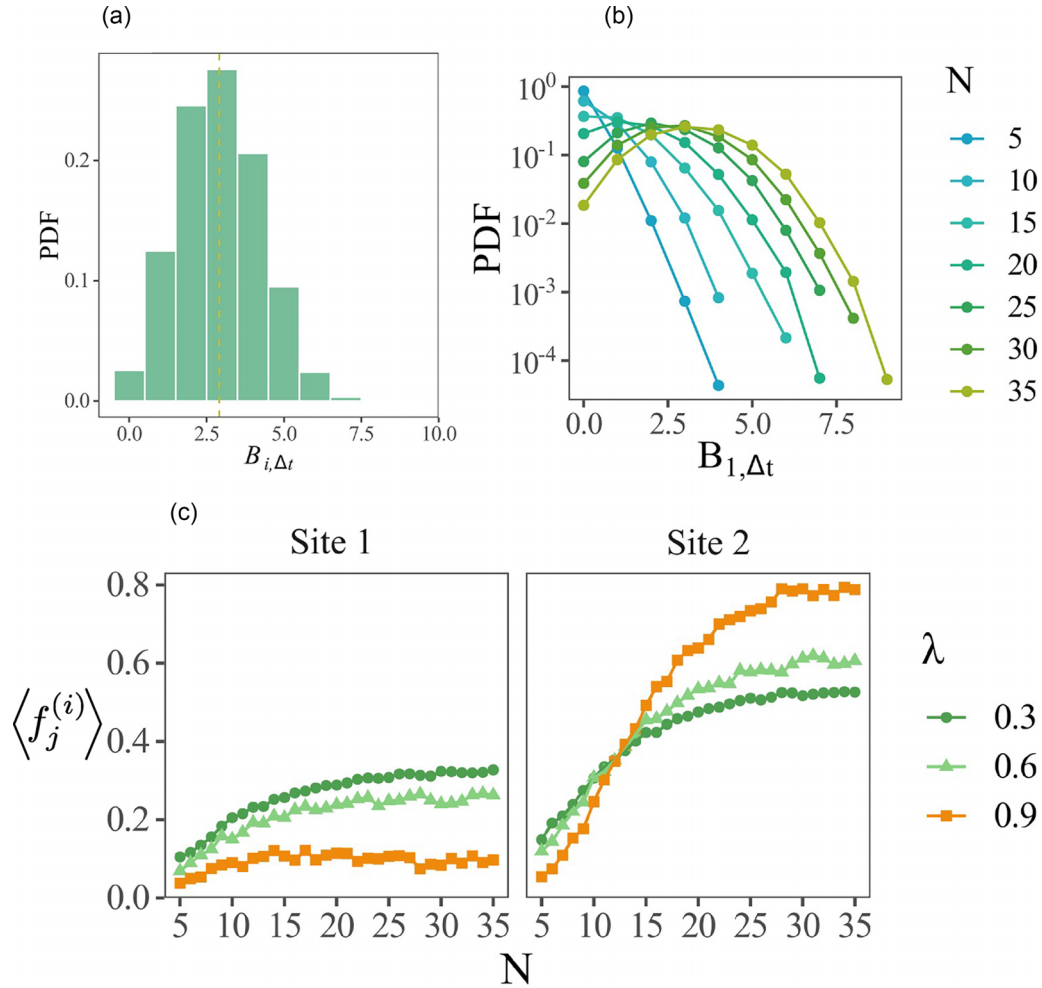


FIG. 12. Kilobots detected during a time step  $\Delta t$  in KILOMBO. (a) Probability distribution,  $B_{i,\Delta t}$ , of kilobots detected by a focal kilobot  $i$  in a time step  $\Delta t$ . (b) Same as A in a logarithmic scale and for different number  $N$  of kilobots in the arena. (c) Average ratio of kilobots dancing for site  $j$  detected by a focal kilobot  $i$  in a time step  $\Delta t$ ,  $f_j^{(i)}$ , as a function of the number  $N$  of kilobots in the arena, for three different values of  $\lambda$ .

Uncommitted bots in KILOMBO detected a mean of  $2.91 \pm 1.35$  bots. With the reassurance that KILOMBO fairly mimics quantitatively the real system, we also analyze how the number of bots seen vary when varying the kilobot density. Figure 12(b) shows the distribution  $B_{i,\Delta t}$ , as the number of kilobots  $N$  goes from  $N = 5$  until  $N = 35$ . As  $N$  increases, curves shift towards the right but, in all cases, the average  $B_{i,\Delta t}$  remains below 5.

The emulator also provides more detailed information about the proportions of detected bots that were dancing for each site. We analyze the ratio of kilobots seen by the focal kilobot  $i$  separating those dancing for each available site  $j$ ,  $f_j^{(i)}$ , during  $\Delta t$  for three contrasting values of the interdependence parameter  $\lambda$ . In Fig. 12(c), we represent the average  $\langle f_j^{(i)} \rangle$  for  $j = 1, 2$  as  $N$  is increased, for  $\lambda = 0.3, 0.6$ , and  $0.9$ . We observe that the  $\langle f_j^{(i)} \rangle$  increase gradually with  $N$  until they reach a plateau for a group of approximately 30 kilobots. As we discuss in the main text, this feature corroborates the existence of a percolating communication network.

## APPENDIX D: COMPLEMENTARY ANALYSIS OF THE COMMUNICATION NETWORK

### 1. Finite-size scaling in quenched configurations

Here we provide a complementary finite-size scaling analysis of communicating cluster formation in quenched configurations of bots randomly located on a circular arena. In Fig. 13(a), we plot the mean-cluster size  $\langle S \rangle$  for different system sizes, preserving the same number density  $N/\pi R^2 = 0.028$  bots/cm<sup>2</sup>, as a function of the communication radius  $r_{\text{int}}$ , which characterizes the maximum extent of message transmission, and thus of information exchange, through infrared sensors among physical kilobots. We can identify the critical percolation interaction radius at around  $r_{\text{int}}^* = 6.5 \pm 0.2$  cm.

Continuous percolation threshold values for two dimensional discs of effective radius  $r_{\text{int}}$  in a square box of linear dimension  $L$  with periodic boundary conditions are found in the literature [77]. The critical filling factor in that particular geometry is  $\eta^* = N\pi r_{\text{int}}^2/L^2 \simeq 1.128$ , or equivalently,  $r_{\text{int}}^* = (L^2\eta^*/(N\pi))^{1/2}$ . Assuming a similar scaling behavior in our

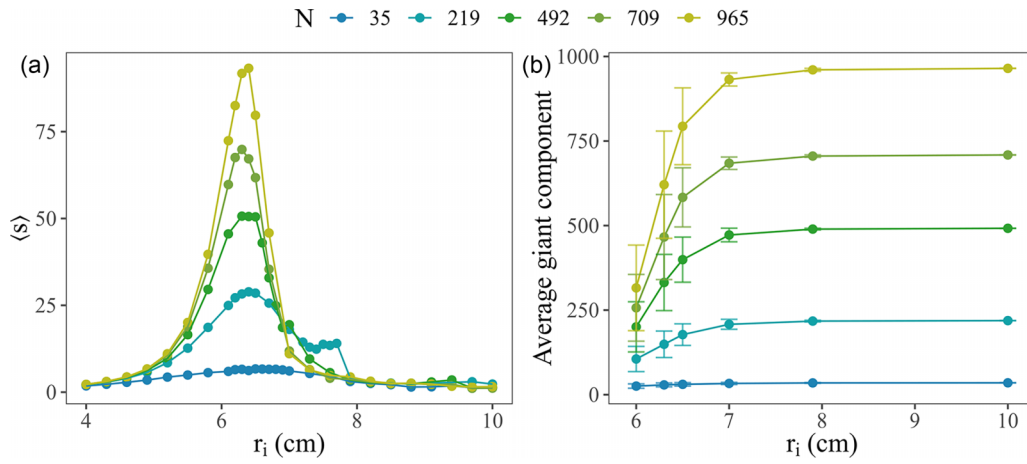


FIG. 13. (a) Mean-cluster size and (b) Average giant component as a function of the communication radius  $r_{int}$  for quenched configurations on different system sizes that preserve the same number density. Cluster sizes were averaged over 1000 configurations per system size.

case, with a fixed rigid circular wall, would yield a smaller threshold radius of approximately 3.59 cm, indicating that both our circular geometry and fixed boundary conditions give rise to packing and size effects that cannot be neglected in the quantitative determination of this nonuniversal threshold value. On the other hand, such effects should not be relevant regarding the behavior of critical exponents.

In Fig. 13(b), we represent the average size of the *giant component* (the largest connected cluster in the system) as a function of the interaction radius  $r_{int}$ . This quantity attains its maximum value, comparable to the system size, after the percolation threshold. As the maximum value of the mean-cluster size, the size of the *giant component* at the percolation threshold scales as a power law of the system size.

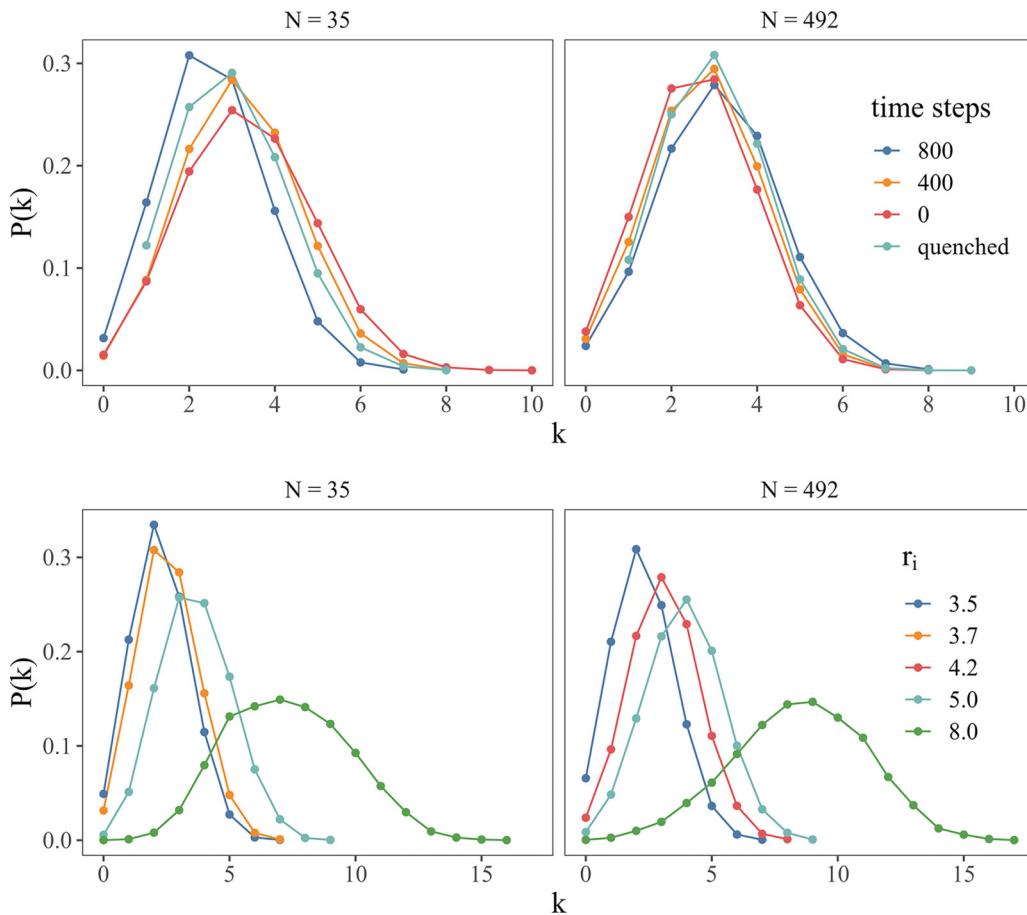


FIG. 14. (Top) Degree distribution  $P(k)$  at the percolation threshold  $r_{int}^*$ . Data obtained from KILOMBO simulations integrating over different time steps,  $\Delta t = 0, 400, 800$  loop iterations and for 1000 quenched bot configurations. (Bottom) Degree distributions obtained for different interaction radius  $r_{int}$  and a fixed value of  $\Delta t = 800$  loop iterations. Left panels correspond to  $N = 35$ , and right panels to  $N = 495$ .

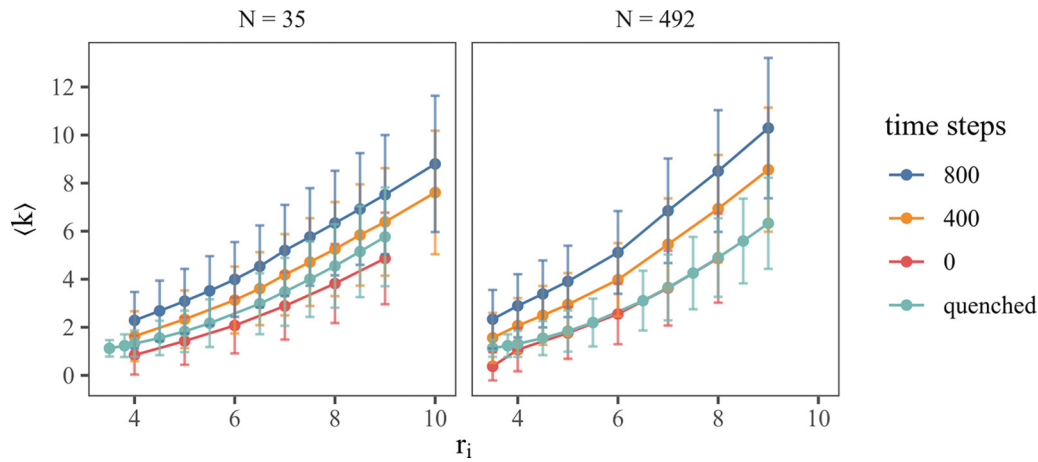


FIG. 15. Average degree  $\langle k \rangle$  of the communication network as a function of  $r_{\text{int}}$ . Results are obtained from KILOMBO simulations integrating over different time steps  $\Delta t = 0, 400, 800$  loop iterations and for 1000 quenched configurations. (Left)  $N = 35$ . (Right)  $N = 492$ .

## 2. Communication network degree distribution

In network theory, a node's degree  $k$  represents its number of connections with other nodes, while the degree distribution  $P(k)$  indicates the probability of a randomly chosen node having degree  $k$  [72]. Both degree and degree distribution are crucial for understanding dynamic processes on networks, such as information spread in the kilobots' infrared communication network.

Figure 14 illustrates the degree distribution observed for the communication network built-up in KILOMBO simulations after integrating over various exploratory time steps ( $\Delta t$ ). Two different system sizes with the same kilobot number density are considered. The bell-shaped curves roughly resemble a Poisson distribution ( $P(k) = e^{-\lambda} \frac{\lambda^k}{k!}$ ), where  $\lambda$  represents the average degree  $\langle k \rangle$ .

Additionally, we compute the average degree ( $\langle k \rangle$ ) of the communication network integrated over different  $\Delta t$  values

in KILOMBO simulations and for quenched random configurations, and the same system sizes ( $N = 35$  and  $492$ ).

Figure 15 shows  $\langle k \rangle$  as a function of  $r_{\text{int}}$  for the same time windows. Increasing  $\Delta t$  and/or interaction radius  $r_{\text{int}}$  results in higher values of  $\langle k \rangle$ , which eventually overcome the threshold average degree  $\langle k \rangle^* = 1$  required for the presence of a giant component in this network according to the celebrated Molloy and Reed criterion [78]. These findings align with a network interpretation of the percolation transition.

For the smaller system ( $N = 35$ ), quenched kilobot configurations exhibit a slightly larger average degree compared to single snapshots of KILOMBO simulations ( $\Delta t = 0$ ), potentially due to the accumulation of some bots at the arena wall. This effect diminishes for the larger system size, yielding similar  $\langle k \rangle$  values for both quenched and  $\Delta t = 0$  configurations.

- [1] T. Bose, A. Reina, and J. A. Marshall, Collective decision-making, *Current Opinion in Behavioral Sciences* **16**, 30 (2017).
- [2] J. R. Dyer, A. Johansson, D. Helbing, I. D. Couzin, and J. Krause, Leadership, consensus decision making and collective behaviour in humans, *Phil. Trans. R. Soc. B* **364**, 781 (2009).
- [3] T. Sasaki and S. C. Pratt, The psychology of superorganisms: Collective decision making by insect societies, *Annu. Rev. Entomol.* **63**, 259 (2018).
- [4] K. von Frisch, *The Dancing Bees* (Springer, Vienna, 1954).
- [5] T. D. Seeley, *Honeybee Democracy* (Princeton University Press, Princeton, NJ, USA, 2010).
- [6] I. D. Couzin, J. Krause, N. R. Franks, and S. A. Levin, Effective leadership and decision-making in animal groups on the move, *Nature (London)* **433**, 513 (2005).
- [7] S. Dong, T. Lin, J. C. Nieh, and K. Tan, Social signal learning of the waggle dance in honey bees, *Science* **379**, 1015 (2023).
- [8] N. F. Britton, N. R. Franks, S. C. Pratt, and T. D. Seeley, Deciding on a new home: how do honeybees agree? *Proc. R. Soc. London B* **269**, 1383 (2002).
- [9] K. M. Passino and T. D. Seeley, Modeling and analysis of nest-site selection by honeybee swarms: the speed and accuracy trade-off, *Behav. Ecol. Sociobiol.* **59**, 427 (2006).
- [10] C. List, C. Elsholtz, and T. D. Seeley, Independence and interdependence in collective decision making: an agent-based model of nest-site choice by honeybee swarms, *Phil. Trans. R. Soc. B* **364**, 755 (2009).
- [11] D. Pais, P. M. Hogan, T. Schlegel, N. R. Franks, N. E. Leonard, and J. A. R. Marshall, A mechanism for value-sensitive decision-making, *PLOS ONE* **8**, 1 (2013).
- [12] A. Reina, J. A. R. Marshall, V. Trianni, and T. Bose, Model of the best-of- $n$  nest-site selection process in honeybees, *Phys. Rev. E* **95**, 052411 (2017).
- [13] R. Gray, A. Franci, V. Srivastava, and N. E. Leonard, Multiagent decision-making dynamics inspired by honeybees, *IEEE Trans. Control Network Syst.* **5**, 793 (2018).
- [14] A. Cavagna, A. Cimarelli, I. Giardina, G. Parisi, R. Santagati, F. Stefanini, and M. Viale, Scale-free correlations in starling flocks, *Proc. Natl. Acad. Sci.* **107**, 11865 (2010).

- [15] S. B. Rosenthal, C. R. Twomey, A. T. Hartnett, H. S. Wu, and I. D. Couzin, Revealing the hidden networks of interaction in mobile animal groups allows prediction of complex behavioral contagion, *Proc. Natl. Acad. Sci. USA* **112**, 4690 (2015).
- [16] D. Chen, T. Vicsek, X. Liu, T. Zhou, and H.-T. Zhang, Switching hierarchical leadership mechanism in homing flight of pigeon flocks, *Europhys. Lett.* **114**, 60008 (2016).
- [17] D. S. Calovi, A. Litchinko, V. Lecheval, U. Lopez, A. Pérez Escudero, H. Chaté, C. Sire, and G. Theraulaz, Disentangling and modeling interactions in fish with burst-and-coast swimming reveal distinct alignment and attraction behaviors, *PLoS Comput. Biol.* **14**, e1005933 (2018).
- [18] J. Múgica, J. Torrents, J. Cristín, A. Puy, M. C. Miguel, and R. Pastor-Satorras, Scale-free behavioral cascades and effective leadership in schooling fish, *Sci. Rep.* **12**, 10783 (2022).
- [19] T. D. Seeley and S. C. Buhrman, Nest-site selection in honey bees: how well do swarms implement the “best-of- $n$ ” decision rule? *Behav. Ecol. Sociobiol.* **49**, 416 (2001).
- [20] G. Valentini, E. Ferrante, and M. Dorigo, The best-of- $n$  problem in robot swarms: Formalization, state of the art, and novel perspectives, *Front. Rob. AI* **4** (2017).
- [21] A. Reina, T. Njougouo, E. Tuci, and T. Carletti, Speed-accuracy trade-offs in best-of- $n$  collective decision making through heterogeneous mean-field modeling, *Phys. Rev. E* **109**, 054307 (2024).
- [22] A. Bizyaeva, A. Franci, and N. E. Leonard, Nonlinear opinion dynamics with tunable sensitivity, *IEEE Trans. Autom. Control* **68**, 1415 (2023).
- [23] S. Garnier, J. Gautrais, M. Asadpour, C. Jost, and G. Theraulaz, Self-organized aggregation triggers collective decision making in a group of cockroach-like robots, *Adapt. Behav.* **17**, 109 (2009).
- [24] H. Hamann, T. Schmickl, H. Wörn, and K. Crailsheim, Analysis of emergent symmetry breaking in collective decision making, *Neural Comput. Appl.* **21**, 207 (2012).
- [25] T. Schmickl, C. Möslinger, and K. Crailsheim, Collective perception in a robot swarm, in *Swarm Robotics*, edited by E. Şahin, W. M. Spears, and A. F. T. Winfield (Springer Berlin Heidelberg, Berlin, Heidelberg, 2007), pp. 144–157.
- [26] G. Valentini, H. Hamann, and M. Dorigo, Self-organized collective decision making: The weighted voter model, in *Proceedings of the 2014 International Conference on Autonomous Agents and Multi-Agent Systems, AAMAS '14* (International Foundation for Autonomous Agents and Multiagent Systems, Richland, SC, 2014), pp. 45–52.
- [27] R. Zakir, M. Dorigo, and A. Reina, Robot swarms break decision deadlocks in collective perception through cross-inhibition, in *Swarm Intelligence: 13th International Conference, ANTS 2022, Málaga, Spain, November 2–4, 2022, Proceedings* (Springer-Verlag, Berlin, Heidelberg, 2022), pp. 209–221.
- [28] R. A. Holley and T. M. Liggett, Ergodic theorems for weakly interacting infinite systems and the voter model, *Ann. Probab.* **3**, 643 (1975).
- [29] C. Castellano, S. Fortunato, and V. Loreto, Statistical physics of social dynamics, *Rev. Mod. Phys.* **81**, 591 (2009).
- [30] S. Galam, Minority opinion spreading in random geometry, *Eur. Phys. J. B* **25**, 403 (2002).
- [31] S. Galam, Sociophysics: A review of galam models, *Int. J. Mod. Phys. C* **19**, 409 (2008).
- [32] G. Deffuant, D. Neau, F. Amblard, and G. Weisbuch, Mixing beliefs among interacting agents, *Adv. Complex Syst.* **03**, 87 (2000).
- [33] S. Redner, Reality-inspired voter models: A mini-review, *C. R. Phys.* **20**, 275 (2019).
- [34] G. De Marzo, A. Zaccaria, and C. Castellano, Emergence of polarization in a voter model with personalized information, *Phys. Rev. Res.* **2**, 043117 (2020).
- [35] A. Franci, A. Bizyaeva, S. Park, and N. E. Leonard, Analysis and control of agreement and disagreement opinion cascades, *Swarm Intelligence* **15**, 47 (2021).
- [36] N. E. Leonard, A. Bizyaeva, and A. Franci, Fast and flexible multiagent decision-making, *Annu. Rev. Control Rob. Auton. Syst.* **7**, 19 (2024).
- [37] A. Reina, G. Valentini, C. Fernandez-Oto, M. Dorigo, and V. Trianni, A design pattern for decentralised decision making, *PLoS ONE* **10**, e0140950 (2015).
- [38] K. Passino, T. Seeley, and P. Visscher, Swarm cognition in honey bees, *Behav. Ecol. Sociobiol.* **62**, 401 (2008).
- [39] V. Trianni, D. De Simone, A. Reina, and A. Baronchelli, Emergence of consensus in a multi-robot network: From abstract models to empirical validation, *IEEE Robot. Autom. Lett.* **1**, 1 (2016).
- [40] G. Valentini, E. Ferrante, H. Hamann, and M. Dorigo, Collective decision with 100 kilobots: speed versus accuracy in binary discrimination problems, *Auton. Agents Multi-Agent Syst.* **30**, 553 (2016).
- [41] A. Reina, T. Bose, V. Trianni, and J. A. R. Marshall, Effects of spatiality on value-sensitive decisions made by robot swarms, in *Distributed Autonomous Robotic Systems: The 13th International Symposium*, edited by R. Groß, A. Kolling, S. Berman, E. Frazzoli, A. Martinoli, F. Matsuno, and M. Gauci (Springer International Publishing, Cham, 2018), pp. 461–473.
- [42] Y. Khaluf, I. Rausch, and P. Simoens, The impact of interaction models on the coherence of collective decision-making: A case study with simulated locusts, in *Swarm Intelligence*, edited by M. Dorigo, M. Birattari, C. Blum, A. L. Christensen, A. Reina, and V. Trianni (Springer International Publishing, Cham, 2018), pp. 252–263.
- [43] C. Dimidov, G. Oriolo, and V. Trianni, Random walks in swarm robotics: An experiment with kilobots, in *Swarm Intelligence*, edited by M. Dorigo, M. Birattari, X. Li, M. López-Ibáñez, K. Ohkura, C. Pinciroli, and T. Stützle (Springer International Publishing, Cham, 2016), pp. 185–196.
- [44] R. A. Johnstone, The evolution of animal signals, in *Behavioural Ecology: An Evolutionary Approach*, edited by J. R. Krebs and N. B. Davies (Blackwell Publishing, Malden, USA, 1997), 4th ed., Chap. 7, pp. 155–178.
- [45] G. F. Golnar, B. Elizabeth, and P. Orit, Data-driven modeling of resource distribution in honeybee swarms, *ALIFE 2023: Ghost in the Machine: Proceedings of the 2023 Artificial Life Conference, Vol. ALIFE 2020: The 2020 Conference on Artificial Life* (2020).
- [46] T. D. Seeley, P. K. Visscher, T. Schlegel, P. M. Hogan, N. R. Franks, and J. A. R. Marshall, Stop signals provide cross inhibition in collective decision-making by honeybee swarms, *Science* **335**, 108 (2012).
- [47] M. Beekman and B. P. Oldroyd, Different bees, different needs: how nest-site requirements have shaped the decision-making

- processes in homeless honeybees (*apis* spp.), *Phil. Trans. R. Soc. B* **373**, 20170010 (2018).
- [48] F. C. Dyer, The biology of the dance language, *Annu. Rev. Entomol.* **47**, 917 (2002).
- [49] T. D. Seeley, Honey bee colonies are group-level adaptive units, *Am. Nat.* **150**, S22 (1997).
- [50] M. R. Myerscough, Dancing for a decision: a matrix model for nest-site choice by honeybees, *Proc. R. Soc. London B* **270**, 577 (2003).
- [51] B. S. Perdriau and M. R. Myerscough, Making good choices with variable information: a stochastic model for nest-site selection by honeybees, *Biology Letters* **3**, 140 (2007).
- [52] T. Galla, Independence and interdependence in the nest-site choice by honeybee swarms: Agent-based models, analytical approaches and pattern formation, *J. Theor. Biol.* **262**, 186 (2010).
- [53] M. Rubenstein, C. Ahler, and R. Nagpal, Kilobot: A low cost scalable robot system for collective behaviors, in *2012 IEEE International Conference on Robotics and Automation* (IEEE, New York, USA, 2012), pp. 3293–3298.
- [54] M. S. Talamali, A. Saha, J. A. R. Marshall, and A. Reina, When less is more: Robot swarms adapt better to changes with constrained communication, *Sci. Robotics* **6**, eabf1416 (2021).
- [55] M. Raoufi, P. Romanczuk, and H. Hamann, Estimation of continuous environments by robot swarms: Correlated networks and decision-making, in *2023 IEEE International Conference on Robotics and Automation (ICRA)* (IEEE, New York, USA, 2023), pp. 5486–5492.
- [56] M. Gauci, R. Nagpal, and M. Rubenstein, Programmable self-disassembly for shape formation in large-scale robot collectives, in *Distributed Autonomous Robotic Systems: The 13th International Symposium*, edited by R. Groß, A. Kolling, S. Berman, E. Frazzoli, A. Martinoli, F. Matsuno, and M. Gauci (Springer International Publishing, Cham, 2018), pp. 573–586.
- [57] I. Slavkov, D. Carrillo-Zapata, N. Carranza, X. Diego, F. Jansson, J. Kaandorp, S. Hauert, and J. Sharpe, Morphogenesis in robot swarms, *Sci. Robotics* **3**, eaau9178 (2018).
- [58] M. Talamali, T. Bose, M. Haire, X. Xu, J. Marshall, and A. Reina, Sophisticated collective foraging with minimalist agents: a swarm robotics test, *Swarm Intelligence* **14**, 25 (2020).
- [59] M. Rubenstein, A. Cabrera, J. Werfel, G. Habibi, J. McLurkin, and R. Nagpal, Collective transport of complex objects by simple robots: Theory and experiments, in *Proceedings of the 2013 International Conference on Autonomous Agents and Multi-Agent Systems, AAMAS '13* (International Foundation for Autonomous Agents and Multiagent Systems, Richland, SC, 2013), pp. 47–54.
- [60] M. Y. B. Zion, J. Fersula, N. Bredeche, and O. Dauchot, Morphological computation and decentralized learning in a swarm of sterically interacting robots, *Sci. Robotics* **8**, eabo6140 (2023).
- [61] F. Jansson, M. Hartley, M. Hinsch, I. Slavkov, N. Carranza, T. S. G. Olsson, R. M. Dries, J. H. Grönqvist, A. F. M. Marée, J. Sharpe, J. A. Kaandorp, and V. A. Grieneisen, Kilombo: a kilobot simulator to enable effective research in swarm robotics, [arXiv:1511.04285](https://arxiv.org/abs/1511.04285) [cs.RO].
- [62] D. Sumpter, The principles of collective animal behaviour, *Phil. Trans. R. Soc. B* **361**, 5 (2006).
- [63] T. M. Judd, The waggle dance of the honey bee: Which bees following a dancer successfully acquire the information? *J. Insect Behav.* **8**, 343 (1994).
- [64] D. March-Pons, E. E. Ferrero, and M. C. Miguel, Consensus formation in quality-sensitive interdependent agent systems, [arXiv:2403.14856](https://arxiv.org/abs/2403.14856) [cond-mat.dis-nn].
- [65] See Supplemental Material at <http://link.aps.org/supplemental/10.1103/PhysRevResearch.6.033149> for this work which contains videos of our experiments.
- [66] A. Reina, T. Bose, V. Trianni, and J. A. R. Marshall, Psychophysical laws and the superorganism, *Sci. Rep.* **8**, 4387 (2018).
- [67] A. Reina, R. Zakir, G. De Masi, and E. Ferrante, Cross-inhibition leads to group consensus despite the presence of strongly opinionated minorities and asocial behaviour, *Commun. Phys.* **6**, 236 (2023).
- [68] F. Peruani and G. J. Sibona, Dynamics and steady states in excitable mobile agent systems, *Phys. Rev. Lett.* **100**, 168103 (2008).
- [69] D. Levis, I. Pagonabarraga, and A. Díaz-Guilera, Synchronization in dynamical networks of locally coupled self-propelled oscillators, *Phys. Rev. X* **7**, 011028 (2017).
- [70] M. Starnini, M. Frasca, and A. Baronchelli, Emergence of metapopulations and echo chambers in mobile agents, *Sci. Rep.* **6**, 31834 (2016).
- [71] M. Paoluzzi, M. Leoni, and M. C. Marchetti, Information and motility exchange in collectives of active particles, *Soft Matter* **16**, 6317 (2020).
- [72] M. Newman, *Networks: An Introduction* (Oxford University Press, Inc., USA, 2010).
- [73] M. Barthélemy, Spatial networks, *Phys. Rep.* **499**, 1 (2011).
- [74] D. Stauffer and A. Aharony, *Introduction to Percolation Theory* (Taylor & Francis, London, UK, 2018).
- [75] T. Aust, M. S. Talamali, M. Dorigo, H. Hamann, and A. Reina, The hidden benefits of limited communication and slow sensing in collective monitoring of dynamic environments, in *Swarm Intelligence*, Lecture Notes in Computer Science, edited by M. Dorigo, H. Hamann, M. López-Ibáñez, J. García-Nieto, A. Engelbrecht, C. Pinciroli, V. Strobel, and C. Camacho-Villalón (Springer International Publishing, Cham, 2022), pp. 234–247.
- [76] Kilocounter, <https://github.com/ivan-paz/kiloColors/blob/main/RGBKiloCounter/>, blob detection and color counting software.
- [77] S. Mertens and C. Moore, Continuum percolation thresholds in two dimensions, *Phys. Rev. E* **86**, 061109 (2012).
- [78] M. Molloy and B. Reed, A critical point for random graphs with a given degree sequence, *Random Struct. Algorithms* **6**, 161 (1995).